

**ORGaNICs: A Theory of Working Memory in Brains and Machines**

David J. Heeger and Wayne E. Mackey

Department of Psychology and Center for Neural Science  
New York University  
4 Washington Place, room 809  
New York, NY 10003

Email: [david.heeger@nyu.edu](mailto:david.heeger@nyu.edu)

Keywords: working memory, LSTM, neural integrator

## Abstract

Working memory is a cognitive process that is responsible for temporarily holding and manipulating information. Most of the empirical neuroscience research on working memory has focused on measuring sustained activity in prefrontal cortex (PFC) and/or parietal cortex during simple delayed-response tasks, and most of the models of working memory have been based on neural integrators. But working memory means much more than just holding a piece of information online. We describe a new theory of working memory, based on a recurrent neural circuit that we call ORGaNICs (Oscillatory Recurrent GAteD Neural Integrator Circuits). ORGaNICs are a variety of Long Short Term Memory units (LSTMs), imported from machine learning and artificial intelligence. ORGaNICs can be used to explain the complex dynamics of delay-period activity in prefrontal cortex (PFC) during a working memory task. The theory is analytically tractable so that we can characterize the dynamics, and the theory provides a means for reading out information from the dynamically varying responses at any point in time, in spite of the complex dynamics. ORGaNICs can be implemented with a biophysical (electrical circuit) model of pyramidal cells, combined with shunting inhibition via a thalamocortical loop. Although introduced as a computational theory of working memory, ORGaNICs are also applicable to models of sensory processing, motor preparation and motor control. ORGaNICs offer computational advantages compared to other varieties of LSTMs that are commonly used in AI applications. Consequently, ORGaNICs are a framework for canonical computation in brains and machines.

## Introduction

Working memory involves much more than simply holding a piece of information online. In the psychology literature, the idea of working memory includes manipulating online information dynamically in the context of new sensory input. For example, understanding a complex utterance (with multiple phrases) often involves disambiguating the syntax and/or semantics of the beginning of the utterance based on information at the end of the sentence. For example, consider the following two sentences:

The athlete realized his goals were unattainable.

The athlete realized his goals quickly.

The first part of each sentence is ambiguous because “his goals” might be the direct object of the verb (as in the second sentence) or the subject of a complement clause (as in the first sentence). Furthermore, one can interpolate any number of modifiers between the ambiguity and the point where it is resolved:

The athlete realized his goals to qualify for this year’s Olympic team (quickly/were unattainable).

Or any number of relative clauses:

The athlete realized his goals which were formed during childhood (quickly/were unattainable).

Comprehending these sentences involves representing and manipulating long-term dependencies, i.e., maintaining a representation of the ambiguous information, and then changing that representation when the ambiguity is resolved.

Most of the empirical neuroscience research on working memory, by contrast, has focused only on maintenance, not manipulation, during delayed-response tasks (Jacobsen, 1935; Fuster and Alexander, 1971; Fuster, 1973). A large body of experimental research has mea-

sured sustained activity in prefrontal cortex (PFC) and/or parietal cortex during the delay periods of various such tasks including memory-guided saccades (e.g., Gnadt and Andersen, 1988; Funahashi et al., 1989; Goldman-Rakic, 1995; Constantinidis et al., 2002; Schluppeck et al., 2006; Srimal and Curtis, 2008) and delayed-discrimination and delayed match-to-sample tasks (e.g., Romo et al., 1999; Hussar and Pasternak, 2012). Most of the models of working memory, based on neural integrators, are aimed to explain sustained delay-period activity or to explain well-established behavioral phenomena associated with sustained activity (Wang, 1999; Compte et al., 2000; Wang, 2001; Wimmer et al., 2014; Almeida et al., 2015). There are, however, a variety of experimental results that are difficult to reconcile with sustained delay-period activity and neural integrator models. First, some (if not the majority of) neurons exhibit complex dynamics during the delay periods, not just constant, sustained activity (Brody et al., 2003; Machens et al., 2005; Shafi et al., 2007; Markowitz et al., 2015; Kobak et al., 2016; Murray et al., 2017). Second, complex dynamics (including oscillations) are evident also in the synchronous activity (e.g., as measured with local field potentials) of populations of neurons (Pesaran et al., 2002; Lundqvist et al., 2016). Third, some of the same neurons exhibit activity that is dependent on task demands (Watanabe, 1996; Platt and Glimcher, 1999; Gold and Shadlen, 2003; Janssen and Shadlen, 2005). Fourth, some of these neurons appear to contribute to different cognitive processes (controlling attention, working memory, decision making, motor preparation, motor control), either for different tasks or during different phases of task execution over time (Quintana and Fuster, 1992; Hasegawa et al., 1998; Rowe et al., 2000; Lebedev et al., 2004; Messinger et al., 2009).

Long Short Term Memory units (LSTMS, Hochreiter and Schmidhuber, 1997) are machine learning (ML) / artificial intelligence (AI) algorithms that are capable of representing and manipulating long-term dependencies, in a manner that is analogous to the concept of working memory in the psychology literature. LSTMs are a class of recurrent neural networks (RNNs). A number of variants of the basic LSTM architecture have been developed and tested for a variety of AI applications. One of the variants, called a gated recurrent unit (GRU), is currently popular (Cho et al., 2014). For a nice introduction to RNNs and LSTMs, see this blog by Christopher Olah:

<http://colah.github.io/posts/2015-08-Understanding-LSTMs/>.

And see this blog by Andrej Karpathy for some demonstrations of AI applications that use RNNs and LSTMs:

<http://karpathy.github.io/2015/05/21/rnn-effectiveness/>

LSTMs have been used for a variety of machine learning problems including language modeling, neural machine translation, and speech recognition (Graves, 2013; Graves et al., 2013; Cho et al., 2014; Graves et al., 2014; Sutskever et al., 2014; Chorowski et al., 2015; Assael et al., 2016; Chan et al., 2016; van den Oord et al., 2016). In these and other tasks, the input stimuli contains information across multiple timescales, but the ongoing presentation of stimuli makes it difficult to correctly combine that information over time (Hochreiter et al., 2001; Pascanu et al., 2013). An LSTM handles this problem by updating its internal state over time with a pair of “gates”: the update gate selects which part(s) of the current input to combine with the current state, and the reset gate selectively deletes part(s) of the current state. The gates are themselves computed from the current inputs and the current outputs. This enables LSTMs to maintain and manipulate a representation of some of the inputs, until needed, without interference from other inputs that come later in time.

Here, we describe a neurobiological theory of working memory, based on a recurrent neural

circuit that we call ORGaNICs (Oscillatory Recurrent GAted Neural Integrator Circuits). The theory is an extension of Heeger’s Theory of Cortical Function (Heeger, 2017), although various complementary approaches have each achieved some of the same goals (O’Reilly and Frank, 2006; Goldman, 2009; Lundqvist et al., 2010; Lundqvist et al., 2011; Costa et al., 2017). ORGaNICs are a variety of LSTMs. Having the capability of an LSTM ensures that the ORGaNICs can solve relatively complicated tasks (much more complicated than the typical delayed-response tasks used in most cognitive psychology and neuroscience experiments). ORGaNICs can exhibit complex dynamics (by using complex-valued weights and responses), but the theory provides a means for “reading out” information from the dynamically varying responses at any point in time, in spite of the complex dynamics.

ORGaNICs can be implemented with a simplified biophysical (equivalent electrical circuit) model of pyramidal cells with separate compartments for the soma, apical dendrite, and basal dendrite. Although introduced as a computational theory of working memory, ORGaNICs are also applicable to models of sensory processing (because deep nets are a special case of stacking ORGaNICs), and motor preparation and motor control (because ORGaNICs may be used to generate signals with complex dynamics, again by using complex-valued weights and responses). ORGaNICs offer computational advantages compared to other varieties of LSTMs that are commonly used in AI applications. Consequently, ORGaNICs are a framework for canonical computation in brains and machines.

## ORGaNICs

The responses of a population of PFC (or parietal) neurons are represented by a vector  $\mathbf{y} = (y_1, y_2, \dots, y_j, \dots, y_N)$  where the subscript  $j$  indexes different neurons in the population. Note that we use boldface lowercase letters to represent vectors and boldface uppercase to denote matrices. The responses  $\mathbf{y}$  depend on an input drive  $\mathbf{z}$  and a recurrent drive  $\hat{\mathbf{y}}$ . The responses  $\mathbf{y}$  are also modulated by two other populations of neurons:  $\mathbf{a}$  and  $\mathbf{b}$ . The variables ( $\mathbf{y}$ ,  $\hat{\mathbf{y}}$ ,  $\mathbf{z}$ ,  $\mathbf{a}$ , and  $\mathbf{b}$ ) are each functions of time, e.g.,  $\mathbf{y}(t)$ , but we drop the explicit dependence on  $t$  to simplify the notation except when it is helpful to disambiguate time steps.

[A note about terminology. We use the term “recurrent”, following the AI and machine literature, to mean feedback processing over time, but the term “recursive” is typically used instead of “recurrent” in the signal processing literature (e.g., recursive filters with infinite impulse responses).]

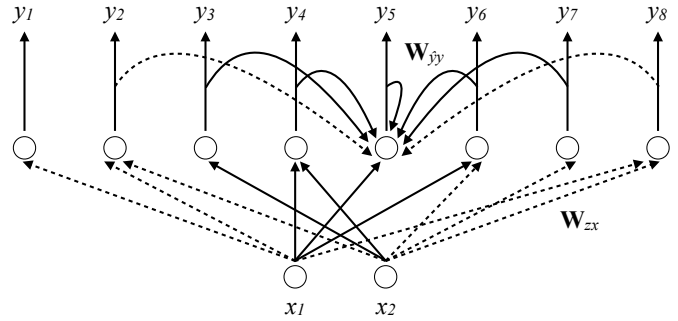
The starting point is the hypothesis that neural responses minimize an energy function that represents a compromise between an input drive and recurrent drive, over time:

$$\begin{aligned} E &= \frac{1}{2} \int \sum_j \left( \frac{b_j^+}{1+b_j^+} \right) [y_j - z_j]^2 + \left( \frac{1}{1+b_j^+} \right) \left[ y_j - \left( \frac{1}{1+\alpha_j^+} \right) \hat{y}_j \right]^2 \\ &\propto \frac{1}{2} \sum_t \sum_j \left( \frac{b_j^+}{1+b_j^+} \right) [y_j - z_j]^2 + \left( \frac{1}{1+b_j^+} \right) \left[ y_j - \left( \frac{1}{1+\alpha_j^+} \right) \hat{y}_j \right]^2 \end{aligned} \quad (1)$$

$$\alpha_j^+ \geq 0 \text{ and } b_j^+ \geq 0 ,$$

where the superscript + is a rectifying output nonlinearity. Halfwave rectification is the simplest form of this rectifying nonlinearity, but other output nonlinearities could be substituted, e.g., sigmoid, exponentiation, half-squaring (Heeger, 1992a), normalization (Heeger, 1992b; Carandini and Heeger, 2012), etc. The second line of Eq. 1 is obtained by discretely sampling time, and the proportionality constant is equal to the time step  $\Delta t$ .

**Figure 1. ORGANIC architecture.** Diagram of connections in an example ORGANIC. Solid lines/curves are excitatory and dashed curves are inhibitory. Only a few of the recurrent connections are shown to minimize clutter. Modulatory connections not shown.



The neural responses are modeled as dynamical processes that minimize the energy  $E$  over time. Taking derivatives of Eq. 1:

$$\begin{aligned} \tau_y \frac{dy_j}{dt} &= -\frac{dE}{dy_j} \\ &= -\left(\frac{b_j^*}{1+b_j^*}\right)\left[y_j - z_j\right] - \left(\frac{1}{1+b_j^*}\right)\left[y_j - \left(\frac{1}{1+\alpha_j^*}\right)\hat{y}_j\right] \\ &= -\left(\frac{b_j^*}{1+b_j^*}\right)y_j + \left(\frac{b_j^*}{1+b_j^*}\right)z_j - \left[1 - \left(\frac{b_j^*}{1+b_j^*}\right)\right]y_j + \left(\frac{1}{1+b_j^*}\right)\left(\frac{1}{1+\alpha_j^*}\right)\hat{y}_j, \\ &= -y_j + \left(\frac{b_j^*}{1+b_j^*}\right)z_j + \left(\frac{1}{1+b_j^*}\right)\left(\frac{1}{1+\alpha_j^*}\right)\hat{y}_j \end{aligned} \quad (2)$$

where  $\tau_y$  is the intrinsic time-constant of the neurons. We note the recurrent drive  $\hat{y}_j(t)$  depends on the responses  $y_j(t-\Delta t)$  from an instant earlier in time, and that the gradient  $dE/dy_j$  is with respect to  $y_j(t)$ , for a specific time  $t$ , so we do not apply the chain rule to  $\hat{y}_j(t)$ .

The input drive depends on a weighted sum of the inputs:

$$\mathbf{z} = \mathbf{W}_{zx}\mathbf{x} + \mathbf{c}_z, \quad (3)$$

where  $\mathbf{x} = (x_1, x_2, \dots, x_j, \dots, x_M)$  is a vector representing the time-varying responses of a population of input neurons. These neurons may also be in PFC, perhaps in the input layer. The encoding matrix (also called the embedding matrix)  $\mathbf{W}_{zx}$  is an  $N \times M$  matrix of weights and  $\mathbf{c}_z$  is an  $N$ -vector of additive offsets. You can think of the rows of  $\mathbf{W}_{zx}$  as being the “receptive fields” of the neurons, and  $\mathbf{c}_z$  as determining the spontaneous firing rates. The weights in  $\mathbf{W}_{zx}$  and the offsets in  $\mathbf{c}_z$  are presumed to be learned, depending on task demands. But the elements of  $\mathbf{W}_{zx}$  and  $\mathbf{c}_z$  were prespecified (not learned), fixed values for each of the simulations in this paper.

The recurrent drive depends on a weighted sum of the responses:

$$\hat{\mathbf{y}} = \mathbf{W}_{\hat{y}y}\mathbf{y} + \mathbf{c}_{\hat{y}}. \quad (4)$$

The recurrent weight matrix  $\mathbf{W}_{\hat{y}y}$  is an  $N \times N$  matrix and  $\mathbf{c}_{\hat{y}}$  an  $N$ -vector of additive offsets. If  $\mathbf{W}_{\hat{y}y}$  is the identity matrix, then each neuron receives a recurrent excitatory connection from itself. If  $\mathbf{W}_{\hat{y}y}$  has a diagonal structure, then each neuron receives recurrent connections from itself and its neighbors. This could, for example, be a center-surround architecture in which the closest recurrent connections are excitatory and the more distant ones are inhibitory.

The readout is also a weighted sum of the responses:

$$\mathbf{W}_{ry}\mathbf{y} + \mathbf{c}_r. \quad (5)$$

where  $\mathbf{W}_{ry}$  is the readout weight matrix (also called the decoding matrix). If  $\mathbf{W}_{ry}$  is the identity

matrix, then the readout is the same as the output responses  $\mathbf{y}$ . The readout may (optionally) be followed by an output nonlinearity, e.g., halfwave rectification, sigmoid, hyperbolic tangent, normalization (Heeger, 1992b; Carandini and Heeger, 2012), etc.

The modulators,  $\alpha$  and  $\mathbf{b}$ , are analogous to the reset gates and update gates, respectively, in a GRU (Cho et al., 2014). The time-varying value of each  $b_j$  determines the effective time-constant of the corresponding response time-course  $y_j$ . The first term of  $E$  (**Eq. 1**) drives the output responses  $\mathbf{y}$  to match the input drive  $\mathbf{x}$ , and the second term drives the output responses to match the recurrent drive  $\hat{\mathbf{y}}$ . Consequently, if  $b_j$  is large then the response time-course  $y_j$  is dominated by the input drive, and if  $b_j$  is small then the response time-course is dominated by the recurrent drive. The time-varying value of  $\alpha_j$  determines the gain of the recurrent drive  $\hat{y}_j$ . If  $\alpha_j$  is large then the recurrent drive is shut down regardless of the value of  $b_j$ .

A (leaky) neural integrator corresponds to the special case in which  $\alpha_j = 0$ ,  $b_j = b$  is the same for all neurons  $j$  and constant over time, and  $\mathbf{c}_z = \mathbf{c}_{\hat{y}} = \mathbf{0}$ . For this special case, we can rewrite **Eq. 2**:

$$\tau_y \frac{dy}{dt} = -\mathbf{y} + \lambda \mathbf{z} + (1 - \lambda) \hat{\mathbf{y}} \quad (6)$$

$$\hat{\mathbf{y}} = \mathbf{W}_{\hat{y}\mathbf{y}} \mathbf{y}$$

$$\lambda = \left( \frac{[b]}{1+[b]} \right) \text{ and } (1 - \lambda) = \left( \frac{1}{1+[b]} \right),$$

where  $0 \leq \lambda \leq 1$ . Even simpler is when  $\mathbf{W}_{\hat{y}\mathbf{y}} = \mathbf{I}$  (where  $\mathbf{I}$  is the identity matrix):

$$\tau_y \frac{dy_j}{dt} = -y_j + \lambda z_j + (1 - \lambda) y_j = \lambda (z_j - y_j) \quad (7)$$

i.e.,

$$\tau'_y \frac{dy_j}{dt} = -y_j + z_j \quad (8)$$

$$\tau'_y = \frac{\tau_y}{\lambda} .$$

where  $\tau_y$  is the intrinsic time-constant and  $\tau'_y$  is the effective time-constant. For this simple special case, each neuron acts like a shift-invariant linear system, i.e., a recursive linear filter with an exponential impulse response function. If the input drive  $z_j$  is constant over time, then the responses  $y_j$  exhibit an exponential time course with steady state  $y_j = z_j$ , and time constant  $\tau'_y$ . This special case reveals how  $\lambda$ , and consequently  $b$  determines the effective time-constant of the leaky integrator.

We introduce a change of variables (from  $\alpha$  to  $\mathbf{a}$ ) in **Eq. 2**:

$$\tau_y \frac{dy_j}{dt} = -y_j + \left( \frac{b_j^+}{1+b_j^+} \right) z_j + \left( \frac{1}{1+a_j^+} \right) \hat{y}_j . \quad (9)$$

For **Eqs. 2** and **9** to be identical:

$$(1+a_j^+) = (1+b_j^+)(1+\alpha_j^+) \quad (10)$$

i.e.,  $a_j^+ = \alpha_j^+ b_j^+ + \alpha_j^+ + b_j^+$ ,

but we will not enforce this constraint, allowing  $a_j$  to take on any value. A leaky integrator now corresponds to the special case in which  $a_j = b_j$ . The original formulation of **Eq. 2** is more elegant because the roles of  $a_j$  and  $b_j$  are distinct:  $a_j$  determines the gain of the recurrent drive and  $b_j$  determines the effective time-constant. But the formulation of **Eq. 9** is more convenient because it has separate modulators,  $a_j$  and  $b_j$ , for the input drive and the recurrent drive, respectively. So we use the formulation of **Eq. 9** in what follows.

**Figure 2. Sustained delay-period activity.**  
**a.** Input (x) corresponding to target presentation. Blue, horizontal position of target. Orange, vertical position. **b.** Input drive. **c, d.** Responses of the modulators, **a** and **b**, analogous to the reset gates and update gates, respectively, in a GRU (Cho et al., 2014). **e.** Output responses (y). **f.** Recurrent weight matrix ( $W_{jy}$ ). The values of the weights range from -0.1213 to 0.3640 (white, positive weights; black, negative weights).

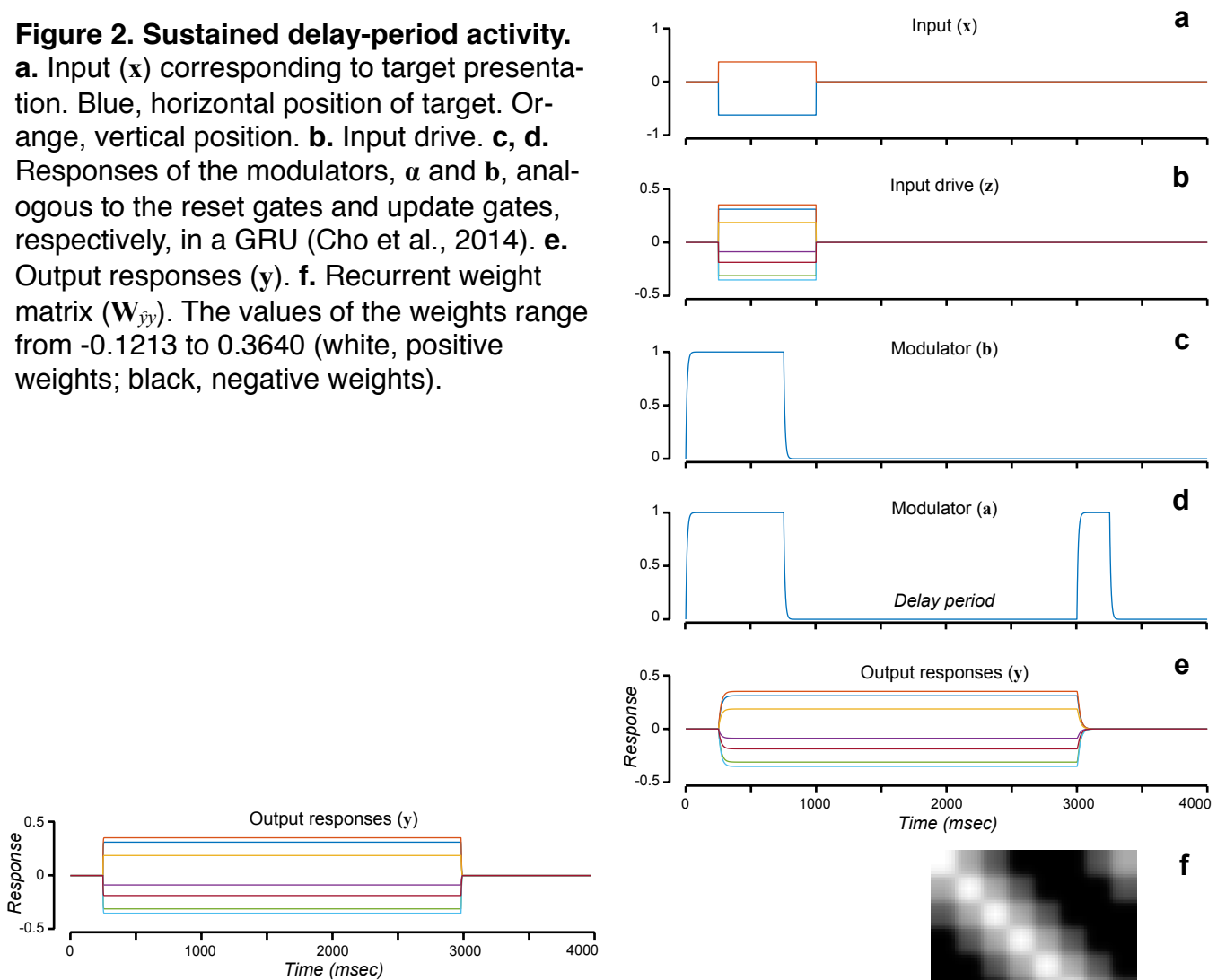


**Figure 3. Sustained delay-period activity, batch algorithm.** Output responses (y) corresponding to the same inputs and weight matrices as in **Fig. 2**.

The modulators **a** and **b** are themselves modeled as dynamical systems that depend on weighted sums of the inputs and outputs:

$$\tau_a \frac{d\mathbf{a}}{dt} = -\mathbf{a} + \mathbf{W}_{ax}\mathbf{x} + \mathbf{W}_{ay}\mathbf{y} + \mathbf{c}_a \quad (11)$$

$$\tau_b \frac{d\mathbf{b}}{dt} = -\mathbf{b} + \mathbf{W}_{bx}\mathbf{x} + \mathbf{W}_{by}\mathbf{y} + \mathbf{c}_b \quad (12)$$

In summary,  $\mathbf{x}$  is a time-varying vector of inputs and  $\mathbf{y}$  is a time-varying vector of output responses. The output responses depend on a weighted sum of the inputs, and a recurrent weighted sum their own responses (an example is depicted in **Fig. 1**). The output responses are also modulated by two time-varying modulators, **a** and **b**, which determine the effective time-constant and the recurrent gain. Each of these modulators depends on a weighted sum of the inputs and outputs. So there are two nested recurrent circuits. First, the responses  $\mathbf{y}$  depend on the recurrent drive ( $\hat{\mathbf{y}}$ ) which depends on a weighted sum of the responses. Second the responses are modulated by a pair of modulators (**a** and **b**), each of which depends on a weighted sum of the responses.

The figures in the following subsections illustrate some of the different operating regimes of ORGaNICs. To briefly preview some of the key results... When  $a_j = b_j > 0$ , the  $j^{\text{th}}$  neuron behaves like a leaky integrator, i.e., a recursive linear filter with an exponential impulse response function. When  $a_j = b_j = 0$ , the response of the  $j^{\text{th}}$  neuron is determined entirely by the recurrent drive and the circuit may exhibit sustained delay-period activity. When  $a_j > b_j$ , the recurrent drive may be shut off (i.e., the neuron's response is reset). When  $b_j > 0$  and  $a_j = 0$ , the neuron behaves like a full (not leaky) integrator. When the eigenvectors and eigenvalues of the recurrent weight matrix are composed of complex values, the responses may exhibit oscillations. Each eigenvector of the recurrent weight matrix is associated with a basis function, a pattern of activity across the population of neurons and over time. The basis functions are damped oscillators when  $\mathbf{a} = \mathbf{b}$ . All this is explained in detail through the examples that follow.

## Implementation

The ORGaNIC algorithm is expressed by the following system of discrete-time equations, looping over  $t$  in increments of  $\Delta t$ :

$$\begin{aligned} \mathbf{z}(t) &= \mathbf{W}_{zx}\mathbf{x}(t) + \mathbf{c}_z \\ \hat{\mathbf{y}} &= \mathbf{W}_{\hat{y}y}\mathbf{y} + \mathbf{c}_{\hat{y}} \\ \Delta\mathbf{a}(t) &= \frac{\Delta t}{\tau_a} \left[ -\mathbf{a}(t) + \mathbf{W}_{ax}\mathbf{x}(t) + \mathbf{W}_{ay}\mathbf{y}(t) + \mathbf{c}_a \right] \\ \mathbf{a}(t + \Delta t) &= \mathbf{a}(t) + \Delta\mathbf{a}(t) \\ \Delta\mathbf{b}(t) &= \frac{\Delta t}{\tau_b} \left[ -\mathbf{b}(t) + \mathbf{W}_{bx}\mathbf{x}(t) + \mathbf{W}_{by}\mathbf{y}(t) + \mathbf{c}_b \right] \\ \mathbf{b}(t + \Delta t) &= \mathbf{b}(t) + \Delta\mathbf{b}(t) \\ \Delta\mathbf{y}_j(t) &= \frac{\Delta t}{\tau_y} \left[ -y_j(t) + \left( \frac{b_j^*(t)}{1+b_j^*(t)} \right) z_j(t) + \left( \frac{1}{1+a_j^*(t)} \right) \hat{y}_j(t) \right] \\ \mathbf{y}(t + \Delta t) &= \mathbf{y}(t) + \Delta\mathbf{y}(t) \end{aligned} \quad (13)$$

The algorithm is incremental, meaning that it stores only a vector of values (one value for each

neuron) for each of the variables: **x**, **y**, **z**, **a**, and **b**. Each of these values is updated during each iteration of the loop from one time point to the next. (Note, however, that we often store these variables as arrays so that we can plot the results over time after finishing the loop).

The example shown in **Fig. 2**, depicts a simulation of the memory-guided saccade task, using the network architecture depicted in **Fig. 1**, with 8 neurons (i.e., **y**, **z**, **a**, and **b** are an 8-dimensional vectors). The input **x** consisted of 4 time courses, the first two of which represented the presentation of the two-dimensional location of a target (**Fig. 2a**; blue, horizontal position; orange, vertical position). Note that the inputs were not selective for saccade amplitude. Instead, the values of these inputs simply increased with the radial position of the target. It would be straightforward to replace these two inputs with a large number of inputs that are each selective for a different two-dimensional location in the visual field. But this 2D input is convenient, because of its much lower dimensionality, for introducing the key concepts of ORGaNICs. The input also consisted of the time-courses of two cues, one of which indicated the beginning of the trial (at time 0 ms) and the other of which indicated the end of the delay period (at time 3000 ms). The input drive (**Fig. 2b**) consisted of 8 time-courses, each of which was responsive to the polar angle location of the target. I.e., the matrix of receptive fields,  $\mathbf{W}_{zx}$ , was an 8x4 matrix:

$$\mathbf{W}_{zx} = \begin{pmatrix} -0.5 & 0 & 0 & 0 \\ -0.3536 & -0.3536 & 0 & 0 \\ 0 & 0.5 & 0 & 0 \\ 0.3536 & 0.3536 & 0 & 0 \\ 0.5 & 0 & 0 & 0 \\ 0.3536 & -0.3536 & 0 & 0 \\ 0 & -0.5 & 0 & 0 \\ -0.3536 & -0.3536 & 0 & 0 \end{pmatrix} \quad (14)$$

The first two columns of  $\mathbf{W}_{zx}$  were, in fact, computed (for reasons explained below) as the first two eigenvectors of the recurrent weight matrix  $\mathbf{W}_{jy}$ . The weight matrices for **a** and **b** were chosen to reflect the other two inputs:

$$\mathbf{W}_{ax} = \begin{pmatrix} 0 & 0 & 1 & 1 \\ 0 & 0 & 1 & 1 \\ 0 & 0 & 1 & 1 \\ 0 & 0 & 1 & 1 \\ 0 & 0 & 1 & 1 \\ 0 & 0 & 1 & 1 \\ 0 & 0 & 1 & 1 \\ 0 & 0 & 1 & 1 \end{pmatrix} \quad \mathbf{W}_{bx} = \begin{pmatrix} 0 & 0 & 1 & 0 \\ 0 & 0 & 1 & 0 \\ 0 & 0 & 1 & 0 \\ 0 & 0 & 1 & 0 \\ 0 & 0 & 1 & 0 \\ 0 & 0 & 1 & 0 \\ 0 & 0 & 1 & 0 \\ 0 & 0 & 1 & 0 \end{pmatrix} \quad (15)$$

Consequently, the response time-courses of **a** and **b** followed the two cues (**Figs. 2c,d**). The recurrent weights  $\mathbf{W}_{jy}$  were chosen to have a center-surround architecture; each row of  $\mathbf{W}_{jy}$  had a large positive value along the diagonal (self-excitation), flanked by smaller positive values, and surrounded by small negative values (**Fig. 2f**). The other weights and offsets were all set to zero:  $\mathbf{W}_{ay}=0$ ,  $\mathbf{W}_{by}=0$ ,  $\mathbf{c}_z=0$ ,  $\mathbf{c}_a=0$ , and  $\mathbf{c}_b=0$ . The responses **y** followed the input drive **z** at the beginning of the simulated trial because **a** and **b** were large (=1, corresponding to a short

effective time constant). The values of **a** and **b** then switched to be small ( $=0$ , corresponding to a long effective time constant) before the target was extinguished, so the output responses **y** exhibited sustained delay-period activity. Finally, the values of **a** were then switched back to be large ( $=1$ , corresponding to a small recurrent gain) at the end of the trial, causing the output responses **y** to be extinguished. Target location was read out (at any time point during the delay period) by multiplying the responses with a pair of readout vectors:

$$\hat{\mathbf{x}} = \mathbf{W}_{ry} \mathbf{y} + \mathbf{c}_r = \mathbf{V}' \mathbf{y} \quad (16)$$

$$\mathbf{V}' = \begin{pmatrix} -0.5 & -0.3536 & 0 & 0.3536 & 0.5 & 0.3536 & 0 & -0.3536 \\ 0 & -0.3536 & 0.5 & 0.3536 & 0 & -0.3536 & -0.5 & -0.3536 \end{pmatrix},$$

where the rows of  $\mathbf{W}_{ry} = \mathbf{V}'$  were (same as the first two columns  $\mathbf{W}_{zx}$ ) computed as the first two eigenvectors of the recurrent weight matrix  $\mathbf{W}_{yy}$ , and  $\mathbf{c}_r = \mathbf{0}$ .

We also implemented a “batch algorithm” that optimizes **Eq. 1** for all time points at once. The batch algorithm is not intended to be a model of neural activity because it requires unlimited memory over time. But it is useful for testing and refining the optimization criterion (**Eq. 1**), and for debugging the incremental algorithm (**Eq. 13**) and the biophysical implementation (**Eqs. 51-65**). The batch algorithm works in two steps (analogous to back-propagation), a forward pass and a backward pass. The forward pass is expressed by the following system of discrete-time equations:

$$\begin{aligned} \mathbf{z}(t) &= \mathbf{W}_{zx} \mathbf{x}(t) + \mathbf{c}_z \\ \hat{\mathbf{y}} &= \mathbf{W}_{\hat{y}y} \mathbf{y} + \mathbf{c}_{\hat{y}} \\ \Delta\mathbf{a}(t) &= \frac{\Delta t}{\tau_a} [-\mathbf{a}(t) + \mathbf{W}_{ax} \mathbf{x}(t) + \mathbf{W}_{ay} \mathbf{y}(t) + \mathbf{c}_a] \\ \mathbf{a}(t + \Delta t) &= \mathbf{a}(t) + \Delta\mathbf{a}(t) \\ \Delta\mathbf{b}(t) &= \frac{\Delta t}{\tau_b} [-\mathbf{b} + \mathbf{W}_{bx} \mathbf{x}(t) + \mathbf{W}_{by} \mathbf{y}(t) + \mathbf{c}_b] \\ \mathbf{b}(t + \Delta t) &= \mathbf{b}(t) + \Delta\mathbf{b}(t) \end{aligned} \quad (17)$$

The backward pass is:

$$\nabla E_j = \frac{\partial E}{\partial y_j(t)} = \left( \frac{b_j^+(t)}{1+b_j^+(t)} \right) (y_j(t) - z_j(t)) + \left( \frac{1}{1+b_j^+(t)} \right) \left( y_j(t) - \left( \frac{1}{1+\alpha_j^+(t)} \right) \hat{y}_j(t) \right) \quad (18)$$

$$\mathbf{y}(t) = \mathbf{y}(t) - r \vec{\nabla} E$$

The algorithm proceeds by alternating between the forward pass and the backward pass. For the batch algorithm, each of **x**, **y**, **z**, **a**, and **b** are stored as arrays (each is a vector for any given time point, over all time points), and the entire array (over all time points) is updated during each iteration. This is different from the incremental algorithm (**Eq. 13**) which stores only a vector of values for each of the variables (**x**, **y**, **z**, **a**, and **b**), each of which is updated with each time step.

The dynamics of the responses (**Fig. 3**) are faster for the batch algorithm (compared to the incremental algorithm) because the batch algorithm does not include a time constant  $\tau_y$  for the output responses.

## Analysis: steady state, readout, and representational dimensionality

The dynamics of the responses depend on the eigenvalues and eigenvectors of the recurrent weight matrix  $\mathbf{W}_{yy}$ . The recurrent weight matrix depicted in **Fig. 2f** serves as a simple example. It is a symmetric, 8x8 matrix (N=8 is the number of neurons in that simple example). Two of the eigenvalues are equal to 1, two of them are 0, and the other 4 have values between 0 and 1. The weight matrix was in fact scaled so that the largest eigenvalues = 1. The corresponding eigenvectors define an orthogonal coordinate system (or basis) for the responses. The responses during the delay period (when  $a=0$ ,  $b=0$ ,  $c_z=0$  and  $c_y=0$ ) are determined entirely by the projection of the initial values (the responses at the very beginning of the delay period) onto the eigenvectors. Eigenvectors with corresponding eigenvalues equal to 1 are sustained throughout the delay period. Those with eigenvalues less than 1 decay to zero (smaller eigenvalues decay more quickly). Those with eigenvalues greater than 1 would be unstable, growing without bound (which is why the weight matrix was scaled so that the largest eigenvalues = 1). So the steady-state responses during the delay period depend on the dot products of the initial responses and the two largest eigenvectors:

$$\mathbf{p} = \mathbf{V}^t \mathbf{y}_0 \quad (19)$$

$$\mathbf{y}_s = \mathbf{V} \mathbf{p} ,$$

where  $\mathbf{y}_s$  is the vector of steady-state responses,  $\mathbf{y}_0$  is the vector of initial values at the beginning of the delay period, the rows of  $\mathbf{V}^t$  were (Eq. 16) computed as the first two eigenvectors of the recurrent weight matrix  $\mathbf{W}_{yy}$ , and  $\mathbf{p}$  is the projection of  $\mathbf{y}_0$  on  $\mathbf{V}$ . The same two eigenvectors were used to encode the input before the delay period:

$$\mathbf{y}_0 = \mathbf{V} \mathbf{x}_0 , \quad (20)$$

where the first two columns of  $\mathbf{W}_{zx}$  are equal to  $\mathbf{V}$ , and  $\mathbf{x}_0$  is a 2x1 vector corresponding to the target position. The same two eigenvectors were used to perform the readout (Eq. 16). Consequently, the readout recovers the input (substituting from **Eqs. 16** and **20** in **Eq. 19**)

$$\hat{\mathbf{x}} = \mathbf{V}^t \mathbf{y}_s = \mathbf{V}^t \mathbf{V} \mathbf{p} = \mathbf{V}^t \mathbf{V} \mathbf{V}^t \mathbf{y}_0 = \mathbf{V}^t \mathbf{V} \mathbf{V}^t \mathbf{V} \mathbf{x}_0 = \mathbf{x}_0 , \quad (21)$$

where the last step simplifies to  $\mathbf{x}_0$  because  $\mathbf{V}$  is an orthonormal matrix (i.e.,  $\mathbf{V}^t \mathbf{V} = \mathbf{I}$ ). The steady-state responses (and consequently the readout) are the same even when the encoding weights (the first two columns of  $\mathbf{W}_{zx}$ ) also include components that are orthogonal to  $\mathbf{V}$ .

Specifically, if the encoding weights are  $\mathbf{V} + \mathbf{V}_p$  such that  $\mathbf{V}^t \mathbf{V}_p = 0$ :

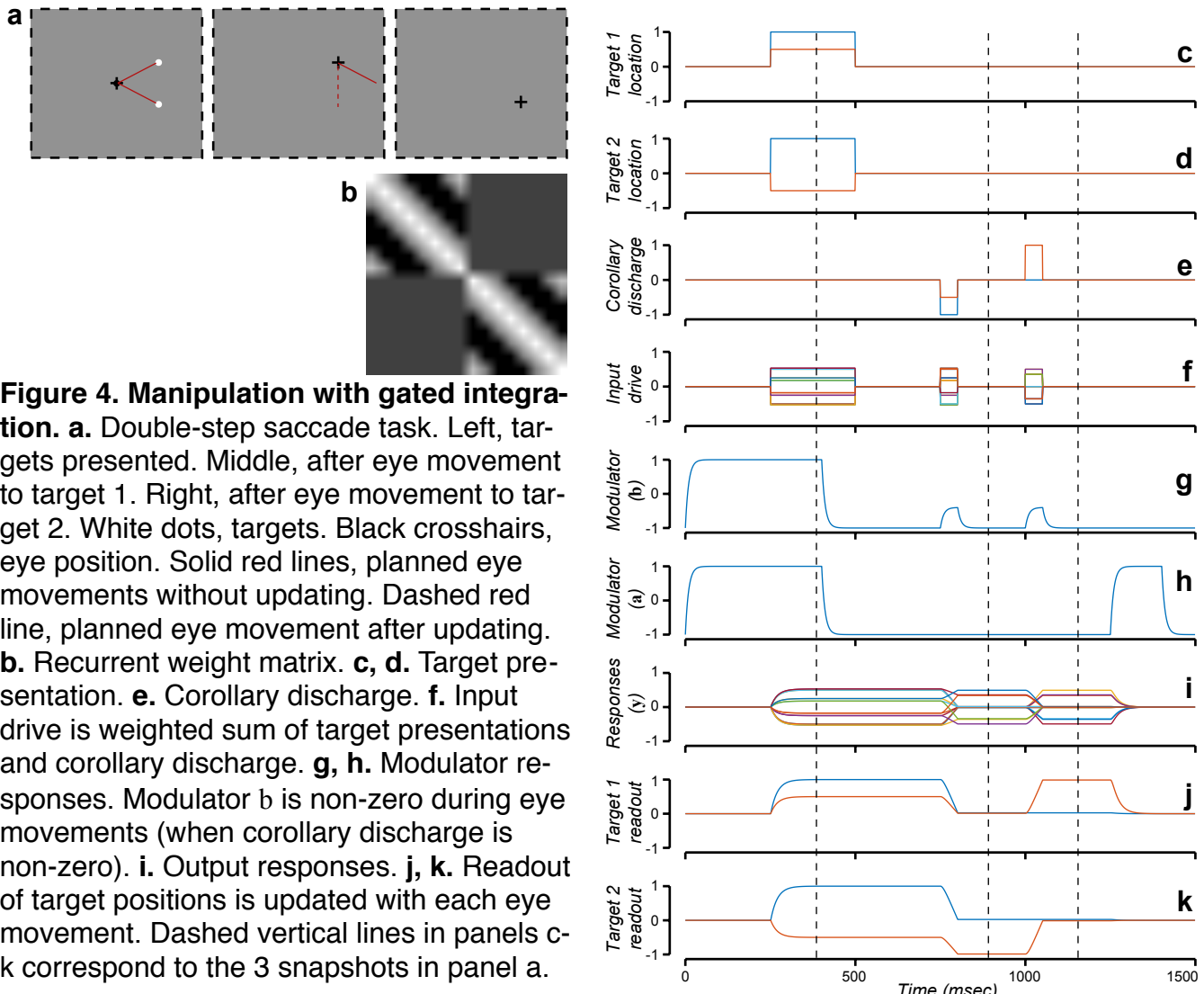
$$\begin{aligned} \mathbf{y}_s &= \mathbf{V} \mathbf{V}^t \mathbf{y}_0 = \mathbf{V} \mathbf{V}^t (\mathbf{V} + \mathbf{V}_p) \mathbf{x}_0 = \mathbf{V} \mathbf{V}^t \mathbf{V} \mathbf{x}_0 = \mathbf{V} \mathbf{x}_0 \\ \hat{\mathbf{x}} &= \mathbf{V}^t \mathbf{y}_s = \mathbf{V}^t \mathbf{V} \mathbf{x}_0 = \mathbf{x}_0 \end{aligned} \quad (22)$$

Likewise, the readout is unaffected by the offsets  $c_z$  and  $c_y$ , when they are orthogonal to  $\mathbf{V}$ .

The example ORGaNIC depicted in **Figs. 1** and **2** has a representational dimensionality  $d = 2$ , because the recurrent weight matrix has two eigenvalues equal to 1. This ORGaNIC is a two-dimensional continuous attractor during the delay period. It can maintain two values, corresponding to the horizontal and vertical locations of the target, where each of those values can be any real number.

## Manipulation via gated integration and reset

Many behavioral tasks and AI applications require manipulation of information (i.e., working



memory) as opposed to maintenance of information (i.e., short-term memory). Such tasks and applications can take full advantage of the computational framework of ORGaNICs (by analogy with LSTMs), which dynamically change state depending on the current input and past context (via **a** and **b**), in which the dependence on past inputs and outputs is controlled separately for each neuron (because the values of **a** and **b** can differ for each neuron). In addition, the encoding and readout weights may have components that are not orthogonal to  $\mathbf{V}$ , the offsets may have components that are not orthogonal to  $\mathbf{V}$ , and the inputs and context may change dynamically before the responses reach steady state. For example, if one of the components of  $\mathbf{c}_y$  is not orthogonal to  $\mathbf{V}$ , then the corresponding component of the responses will reflect the elapsed time interval since the beginning of the delay period (i.e., it behaves like a neural integrator).

A simulation of the double-step saccade task illustrates how ORGaNICs can both maintain and manipulate information over time (**Fig. 4**). In this task, two targets are shown while a subject is fixating the center of a screen (**Fig. 4a**, left panel). A pair of eye movements are then made in sequence to each of the two targets. Eye movements are represented in the brain using retinotopic, i.e., eye-centered coordinates (**Fig. 4a**, left panel, red lines). But after making the first eye movement, the plan for the second eye movement must be updated (**Fig. 4b**, middle panel, solid red line copied from left panel no longer points to the second target). This is

done by combining a representation of the target location with a copy of the neural signals that control the eye muscles (called corollary discharge) to update the planned eye movement (**Fig. 4b**, middle panel, dashed red line). The ORGaNIC in **Fig. 4** received two types of inputs: 1) the target locations (**Fig. 4c,d**), and 2) the corollary discharge (**Fig. 4e**). The encoding weight matrix transformed the target positions to the responses of a network of 16 neurons (8 for each target). As in **Fig. 2**, the responses  $y$  followed the input drive  $z$  at the beginning of the simulated trial because  $a$  and  $b$  were large ( $=1$ , corresponding to a short effective time constant). The values of  $a$  and  $b$  were then switched to be small ( $=0$ , corresponding to a long effective time constant) before the targets were extinguished, so the output responses  $y$  exhibited sustained delay-period activity that represented the original target locations (**Fig. 4c-k**, leftmost vertical dashed line). Finally, the values of  $a$  were then switched back to be large ( $=1$ , corresponding to a small recurrent gain) at the end of the trial, causing the output responses  $y$  to be extinguished. The modulators  $b$  were non-zero during eye movements (**Fig. 4g**), when the corollary discharge was non-zero (**Fig. 4c**), so that the responses  $y$  integrated the corollary discharge with the stored representation of the target locations. The last two panels (**Fig. 4j,k**) show the readout of each of the two target locations over time. Preceding the first eye movement (**Fig. 4j,k**, leftmost dashed line), the responses encoded the original target locations: (1, 0.5) and (-1, 0.5). After the first eye movement (**Fig. 4j,k**, middle dashed line), the responses encoded the corresponding updated target locations: (0, 0) and (0, -1). After the second eye movement (**Fig. 4j,k**, rightmost dashed line), the responses were updated again to encode correspondingly updated target locations: (0, 1) and (0, 1). The corollary discharge (**Fig. 4e**) was simply a copy of the readout from just before the corresponding eye movement, i.e., from **Fig. 4j** just before the first eye movement and from **Fig. 4k** just before the second eye movement.

## Oscillatory activity

The same computational framework can be used to generate delay-period activity with complex dynamics, rather than just sustained activity, and the same theoretical framework can be used to analyze it. The key idea is that the weights and the output responses may be complex-valued. The complex-number notation is just a notational convenience. The complex-valued responses may be represented by pairs of neurons, and the complex-valued weights in the recurrent weight matrix may be represented by pairs of synaptic weights.

A recurrent weight matrix in the form of a synfire chain (Abeles, 1982), for example, generates periodic activity (**Fig. 5**). The example network depicted in **Fig. 5** has 100 neurons, the recurrent weight matrix  $\mathbf{W}_{yy}$  (a 100x100 matrix) contains 0's along the main diagonal and 1's along the diagonal adjacent to the main diagonal (**Fig. 5a**), looping back from the 100<sup>th</sup> neuron to the 1<sup>st</sup> neuron (**Fig. 5a**, top-right). Consequently, the activity is “handed off” from one neuron to the next during a delay period. The encoding matrix is 100x4. Otherwise, this example network is the same as that depicted in **Figs 1** and **2**. The responses are complex-valued and oscillatory during the delay period (**Fig. 5b**).

The dynamics of the responses during the delay period again depend on the eigenvalues and eigenvectors of recurrent weight matrix  $\mathbf{W}_{yy}$ . For this recurrent weight matrix, the eigenvectors and eigenvalues are complex-valued. Two of the eigenvalues have real parts equal to 1. The rest of the eigenvalues have real parts that are less than 1 (some of them being negative). The components of the responses corresponding to the 98 eigenvalues with real parts that are less than 1 decay to 0 during a delay period, so only the first two components are relevant for the steady-state responses. The imaginary parts of the first two eigenvalues determine the os-

**Figure 5. Periodic dynamics with synfire chain recurrent weights. a.** Recurrent weight matrix ( $\mathbf{W}_{yy}$ ).  $N=100$ ;  $d=2$ . **b.** Output responses ( $\mathbf{y}$ ). Upper panel, real part of the complex-valued responses. Lower panel, imaginary part. Only a small fraction of the 100 response time-courses are shown in each panel.

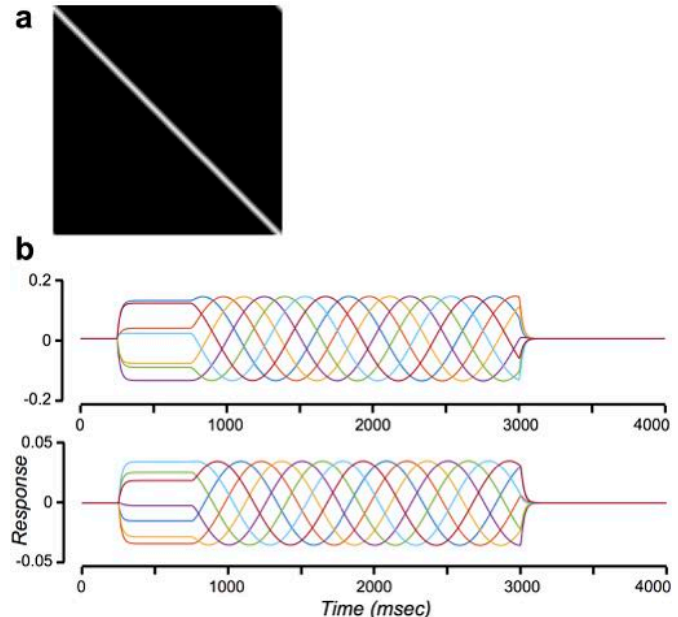
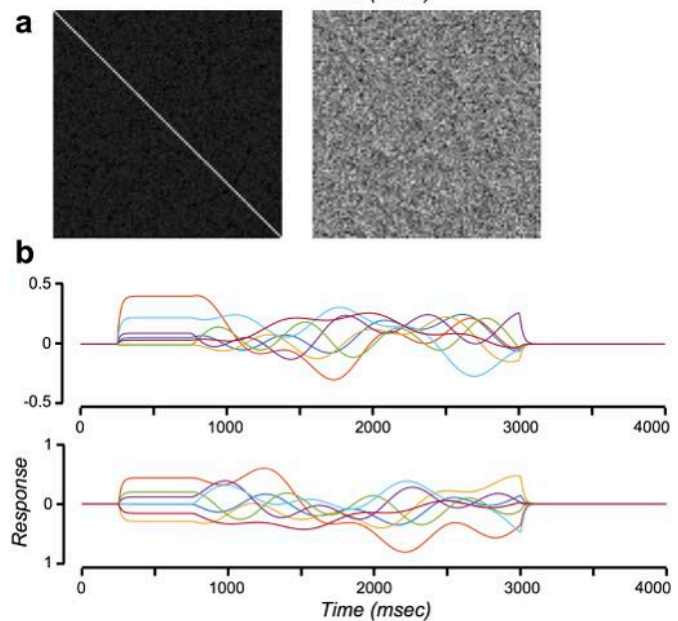


**Figure 6. Delay-period dynamics with general recurrent weights. a.** Recurrent weight matrix ( $\mathbf{W}_{yy}$ ). Left, real part of the complex-valued weight matrix (values of the weights range from -0.1 to 0.7; white, positive weights; black, negative weights). Right, imaginary part (values of the weights range from -0.1 to 0.1; white, positive weights; black, negative weights). **b.** Output responses ( $\mathbf{y}$ ). Upper panel, real part of the complex-valued responses. Lower panel, imaginary part. Only a small fraction of the 100 response time-courses are shown in each panel.



cillation frequencies. In this example, the imaginary parts are small ( $\pm 0.0629$ ), corresponding to a slow frequency. In fact, the period of oscillation is 1 sec because there are 100 neurons in the synfire chain, each with an intrinsic time-constant  $\tau_y = 10$  ms. In spite of the oscillations, target location may be read out (up to a sign change), at any time point during the delay period, by multiplying the responses with a pair of readout vectors:

$$\hat{\mathbf{x}} = |\mathbf{V}' \mathbf{y}| = |\mathbf{x}_0| , \quad (23)$$

where the superscript  $\prime$  now means conjugate transpose, the rows of  $\mathbf{V}'$  are once again the same as the first two columns of the encoding matrix  $\mathbf{W}_{zx}$ , computed as the first two (complex-valued) eigenvectors of the recurrent weight matrix  $\mathbf{W}_{yy}$ . Only the absolute value of the input can be read out (i.e., up to a sign change) using Eq. 23, because the responses oscillate over time with a combination of frequency components (depending on the imaginary parts of the eigenvectors), and the frequencies, phases, and elapsed time are presumed to be unknown. The sign may be resolved if the frequencies, phases, and elapsed time are known.

A further generalization is depicted in **Fig. 6**, which exhibits complex dynamics. Once again, in spite of the complex dynamics, target location may be read out (up to a sign change), at any point during the delay period (**Eq. 23**). In this example, there are again 100 neurons and the recurrent weight matrix  $\mathbf{W}_{yy}$  is a 100x100 matrix. The recurrent weight matrix was designed to have real parts of 10 eigenvalues equal to 1, real parts of the other 90 eigenvalues less than 1, and with small imaginary parts (between -0.1 and 0.1) for all 100 eigenvalues. Consequently, the steady-state responses have a representational dimensionality of  $d = 10$ ,  $\mathbf{V}$  is a 100x10 matrix containing 10 eigenvectors, and  $\mathbf{W}_{zx}$  is a 100x12 matrix (10 dimensions plus 2 cues).

The recurrent weight matrix was created using the following algorithm. First, we filled a 100x100 matrix  $\mathbf{A}$  with random complex-valued numbers (normally distributed with mean 0 and standard deviation 1). Second, we computed the QR decomposition of the matrix  $\mathbf{A}$ , yielding a unitary matrix of complex-valued numbers  $\mathbf{Q}$ , such that  $\mathbf{Q}' \mathbf{Q} = \mathbf{Q} \mathbf{Q}' = \mathbf{I}$ . Third, we created a diagonal matrix  $\mathbf{D}$  with the desired eigenvalues, with real parts equal to 1 for 10 of them and random numbers (uniformly distributed between 0 and 1) for the rest, and with random imaginary parts (normally distributed with mean 0 and standard deviation 0.05). Again, the imaginary parts of the eigenvalues were purposefully chosen to be small so that the oscillation frequencies would be low. Finally, we multiplied  $\mathbf{W}_{yy} = \mathbf{Q} \mathbf{D} \mathbf{Q}'$ , similar to reconstructing a matrix from its singular-value decomposition.

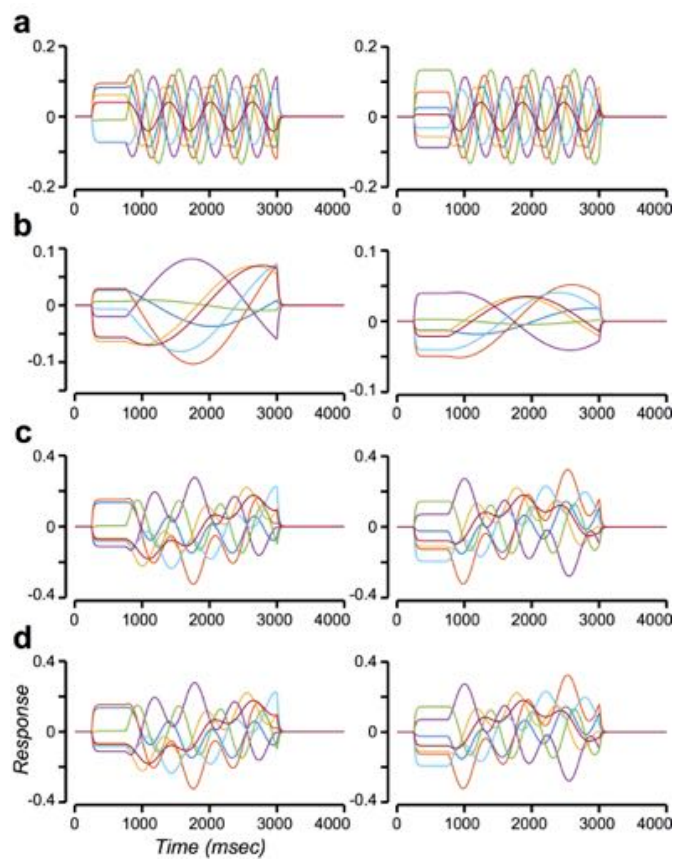
This example ORGaNIC has a representational dimensionality  $d = 10$ , because the recurrent weight matrix was constructed to have 10 eigenvalues with real parts equal to 1. It is a ten-dimensional continuous attractor during the delay period, and it can maintain ten values (e.g., the horizontal and vertical locations of 5 targets). In the preceding examples (**Figs. 2** and **4**, with center-surround recurrent weights or synfire weights, respectively), the recurrent weight matrices have only 2 eigenvalues with real parts equal to 1, so the representational dimensionality of those ORGaNICs is only 2.

### Signal generators, motor preparation, and motor control

ORGaNICs are also capable of generating signals, like that needed to execute a complex sequence of movements (e.g., bird song, speech generation, golf swing, bowling, skiing moguls, backside double McTwist 1260 on a snowboard out of the halfpipe). Some actions are ballistic (open loop), meaning that they are executed with no sensory feedback. Others are closed loop, meaning that the movements are adjusted on the fly based on sensory feedback. ORGaNICs can produce patterns of activity over time that might underlie the execution of both open- and closed-loop movements.

Open-loop control corresponds to the delay-period responses described above. Each eigenvector of the recurrent weight matrix is associated with a basis function, a pattern of activity across the population of neurons and over time. The basis functions are complex exponentials (sines and cosines) when the modulators ( $\mathbf{a}$  and  $\mathbf{b}$ ) are 0. Examples of these basis functions are plotted in **Fig. 7a,b**. The time course of the input, and the time courses of the modulators ( $\mathbf{a}$  and  $\mathbf{b}$ ) were the same in this simulation as in **Figs. 2-5**, and the recurrent weight matrix was the same as that shown in **Fig. 5a**. When the input drives only a single eigenvector (i.e., because the input is orthogonal to the other eigenvectors), then the responses during the delay period (when  $\mathbf{a} = \mathbf{b} = \mathbf{0}$ ) are sinusoidal, all with the same frequency (as determined by the imaginary part of the corresponding eigenvalue). But the response of each neuron, in general, exhibits a different amplitude and phase (**Fig. 7a**). When the input drives another eigenvector, then the neurons exhibit responses with a different temporal frequency (**Fig. 7b**). A linear sum

**Figure 7. Signal generators for motor preparation and motor control.** **a.** Response time-series when input (with amplitude = 1) drives only one of the eigenvectors of the recurrent weight matrix ( $\mathbf{W}_{\hat{y}\hat{y}}$ ). Left panel, real part of the complex valued responses ( $y$ ). Right panel, imaginary part of the complex-valued responses. **b.** Response time-series when input drives a second eigenvector. Same format as panel a. **c.** Response time course driven by a linear combination of the inputs in panels a and b. **d.** Linear combination of the responses from panels a and b. The curves in panel d are identical those in panel c because the responses behave like a linear system; a linear sum of the inputs evokes a linear sum of the responses. Only a small fraction of the 100 response time-courses are shown in each panel.



of the inputs evokes a linear sum of the responses (compare **Fig. 7c** and **Fig. 7d**). Linear sums of these sinusoidal basis functions may be used as control signals for ballistic (open loop) movements.

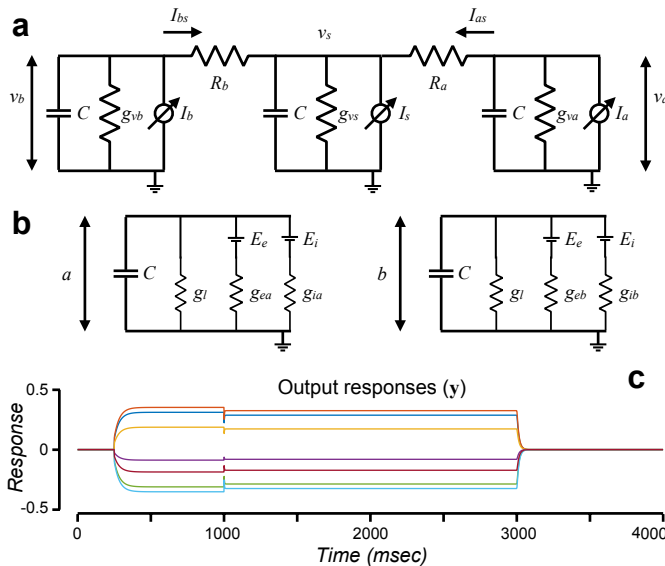
The readout for open-loop control is, in general, an arbitrary linear transform of the responses:  $\mathbf{W}_{ry} y$  (optionally followed by an output nonlinearity). The readout matrix for short-term memory, as discussed above, may be comprised of the eigenvectors of the recurrent weight matrix. Doing so ensures that the input is recovered (up to a sign change) at any time during the delay period. But recovering the input is not the goal for open-loop control.

The basis functions are damped oscillators when the modulators are greater than 0 but equal to one another (**a** = **b**) and constant over time, and when the input is constant over time.

If the input is varying over time, then the responses depend on a linear combination of the inputs and the basis functions, and the responses may be used for closed-loop control. If the modulators (**a** and **b**) are also time-varying, then the closed-loop control responses may exhibit a wide range of complex dynamics.

### Biophysical implementation

In this section, we describe a possible biophysical implementation of ORGaNICs (**Fig. 8**). The key idea is that the two terms corresponding to the input drive and recurrent drive are computed in separate dendritic compartments of a cortical pyramidal cell. First, we hypothesize that the input drive  $z$ , modulated by **b**, is computed in the soma and basal dendrites. Second, we hypothesize that the recurrent drive  $\hat{y}$ , modulated by **a**, is computed in the apical dendrites. Furthermore, we assert, based on experimental evidence (Fuster and Alexander, 1971; Guo et al., 2017; Schmitt et al., 2017), that the modulatory responses corresponding to the modulators, **a** and **b**, are computed in the thalamus.



The analysis relies on an equivalent circuit model of a pyramidal cell. Heeger's lecture notes provide an introduction to how we approach neural computation with equivalent circuit models:

<http://www.cns.nyu.edu/~david/handouts/membrane.pdf>

<http://www.cns.nyu.edu/~david/handouts/synapse.pdf>

A simplified electrical-circuit model of a pyramidal cell is depicted in **Fig 7a**. The model comprises 3 compartments for the soma, the apical dendrite, and the basal dendrite. Each compartment is an RC circuit with a variable-conductance resistor and a variable current source. The capacitors represent the electrical capacitance of the neural membrane. Each current source approximates a combination of excitatory and inhibitory synaptic inputs (see lecture notes, above). Each variable-conductance resistor ( $g_{va}$ ,  $g_{vb}$ , and  $g_{vs}$ ) represents shunting synaptic input. The two fixed-conductance resistors labeled  $R_a$  and  $R_b$  represent the resistances between the compartments (i.e., along the dendritic shafts).

### Pyramidal cell model

To analyze the function of this electrical-circuit model, we express the somatic membrane potential as a function of the synaptic inputs (the variable conductance resistors and the current sources in each compartment). To simplify the derivation, without loss of generality, we set the resting membrane potential (corresponding to when there is no synaptic input) to 0. (For a non-zero resting potential, we could simply add a voltage source, i.e., battery, equal to the resting potential, in series with variable-conductance resistors in each compartment.) From Kirchhoff's current law:

$$C \frac{dv_a}{dt} + g_{va} v_a - I_a + I_{as} = 0 \quad (24)$$

$$C \frac{dv_b}{dt} + g_{vb} v_b - I_b + I_{bs} = 0 \quad (25)$$

**Figure 8. Biophysical implementation.** **a.** Electrical-circuit model of a pyramidal cell with separate RC circuit compartments for the soma, the apical dendritic tree, and the basal dendritic tree.  $g_{va}$ ,  $g_{vb}$ , shunting synapses represented by variable conductance resistors.  $I_a$ ,  $I_b$ , synaptic input represented by variable current sources.  $v_s$ , somatic membrane potential.  $v_a$ ,  $v_b$ , membrane potentials, respectively, in apical and basal dendrites.  $C$ , membrane capacitance. **b.** Electrical-circuit models of thalamic cells corresponding to the modulators.  $a$ ,  $b$ , membrane potentials of two neurons corresponding to the two modulators.  $g_{ea}$ ,  $g_{eb}$ , excitatory synaptic conductances.  $g_{ia}$ ,  $g_{ib}$ , inhibitory synaptic conductances.  $E_e$ , reversal potential of excitatory synapses.  $E_i$ , reversal potential of inhibitory synapses.  $g_l$ , leak conductance. **c.** Output responses ( $y$ ) corresponding to the same inputs and weight matrices as in **Fig. 2**.

**2. Model parameters:**  $C = 1$ ;  $g_{vs} = 1$ ;  $R_a = 10$ ;  $R_b = 1$ ;  $g_l = 1$ .

$$C \frac{dv_s}{dt} + g_{vs}v_s - I_s - I_{as} - I_{bs} = 0 \quad . \quad (26)$$

The membrane potentials  $v_s$ ,  $v_a$ , and  $v_b$  correspond to the soma, the apical dendrite, and the basal dendrite, respectively. The currents flowing from the soma, and from each of the dendrites, to the extracellular space are denoted  $I_s$ ,  $I_a$ , and  $I_b$ . The internal currents flowing between compartments are denoted  $I_{as}$  and  $I_{bs}$ . In addition, from Ohm's Law:

$$v_a - v_s = R_a I_{as} \quad (27)$$

$$v_b - v_s = R_b I_{bs} \quad . \quad (28)$$

Substituting for  $I_{as}$  and  $I_{bs}$  in Eq. 26 from Eqs. 24 and 25:

$$\left( C \frac{dv_s}{dt} + g_{vs}v_s - I_s \right) + \left( C \frac{dv_a}{dt} + g_{va}v_a - I_a \right) + \left( C \frac{dv_b}{dt} + g_{vb}v_b - I_b \right) = 0 \quad . \quad (29)$$

The steady-state values for the membrane potentials and internal currents, assuming that the synaptic inputs are constant over time, are derived by setting the derivatives equal to zero in Eqs. 24, 25, and 29:

$$-g_{va}v_a + I_a = I_{as} \quad (30)$$

$$-g_{vb}v_b + I_b = I_{bs} \quad (31)$$

$$g_{vs}v_s - I_s + g_{va}v_a - I_a + g_{vb}v_b - I_b = 0 \quad . \quad (32)$$

Substituting for the internal current  $I_{as}$  from Eq. 30 into Eq. 27:

$$\begin{aligned} v_a - v_s &= R_a I_{as} \\ v_a - v_s &= R_a (I_a - g_{va}v_a) \\ v_a + R_a g_{va}v_a &= v_s + R_a I_a \\ (1 + R_a g_{va})v_a &= v_s + R_a I_a \\ v_a &= \frac{v_s + R_a I_a}{1 + R_a g_{va}} = \frac{v_s}{1 + R_a g_{va}} + \frac{R_a I_a}{1 + R_a g_{va}} \end{aligned} \quad . \quad (33)$$

Likewise, substituting for the internal currents  $I_{bs}$  from Eq. 31 into Eq. 28:

$$v_b = \frac{v_s}{1 + R_b g_{vb}} + \frac{R_b I_b}{1 + R_b g_{vb}} \quad . \quad (34)$$

Substituting for  $v_a$  and  $v_b$  from Eqs. 33-34 into Eq. 32:

$$\begin{aligned} g_{vs}v_s - I_s + \frac{g_{va}}{1 + R_a g_{va}}v_s + \frac{R_a g_{va}}{1 + R_a g_{va}}I_a - I_a + \frac{g_{vb}}{1 + R_b g_{vb}}v_s + \frac{R_b g_{vb}}{1 + R_b g_{vb}}I_b - I_b &= 0 \\ v_s \left( g_{vs} + \frac{g_{va}}{1 + R_a g_{va}} + \frac{g_{vb}}{1 + R_b g_{vb}} \right) &= I_s + I_a \left( 1 - \frac{R_a g_{va}}{1 + R_a g_{va}} \right) + I_b \left( 1 - \frac{R_b g_{vb}}{1 + R_b g_{vb}} \right) \\ v_s \left( g_{vs} + \frac{g_{va}}{1 + R_a g_{va}} + \frac{g_{vb}}{1 + R_b g_{vb}} \right) &= I_s + \left( \frac{1}{1 + R_a g_{va}} \right) I_a + \left( \frac{1}{1 + R_b g_{vb}} \right) I_b \end{aligned} \quad (35)$$

Eq. 35 is a general expression for the steady-state somatic membrane potential  $v_s$  in terms of

the synaptic inputs ( $I_s$ ,  $I_a$ ,  $I_b$ ,  $g_{va}$ ,  $g_{vb}$ , and  $g_{vs}$ ) and the fixed (constant) resistances along the dendrites ( $R_a$  and  $R_b$ ).

To implement ORGaNICs with this pyramidal-cell model, we specify the synaptic inputs ( $I_s$ ,  $I_a$ ,  $I_b$ ,  $g_{va}$ ,  $g_{vb}$ , and  $g_{vs}$ ) to each neuron in terms of its input drive ( $y$ ), recurrent drive ( $\hat{y}$ ), modulators ( $a$  and  $b$ ):

$$\begin{aligned} g_{va}(t) &= \frac{1}{R_a} a^+(t) \\ g_{vb}(t) &= \frac{1}{R_b} b^+(t) \\ I_s(t) &= z(t) \\ I_b(t) &= -z(t) \\ I_a(t) &= \hat{y}(t) = y^+(t) - y^-(t) \end{aligned} \quad (36)$$

and where  $g_{vs}$  is presumed to be a constant. We presume that the output firing rate is well-approximated by halfwave rectification:

$$y^+(t) = \lfloor v_s(t) \rfloor, \quad (37)$$

and that the negative values (corresponding to hyperpolarization of the membrane potential  $v_s$ ) are represented by a separate neuron that receives the complementary synaptic inputs (identical for  $g_{va}$  and  $g_{vb}$ , and opposite in sign for  $I_s$ ,  $I_a$ , and  $I_b$ ), analogous to ON- and OFF-center retinal ganglion cells. Substituting from **Eq. 36** into **Eq. 35**

$$v_s \left( g_{vs} + \frac{a^+}{R_a(1+a^+)} + \frac{b^+}{R_b(1+b^+)} \right) = z + \frac{1}{1+a^+} \hat{y} - \frac{1}{1+b^+} z, \quad (38)$$

$$g_v v_s = \frac{b^+}{1+b^+} z + \frac{1}{1+a^+} \hat{y}, \quad (39)$$

where  $g_v$  is the total synaptic conductance:

$$g_v = g_{vs} + \frac{a^+}{R_a(1+a^+)} + \frac{b^+}{R_b(1+b^+)} . \quad (40)$$

The steady-state membrane potential (**Eq. 39**) is a weighted sum of the input drive and recurrent drive, modulated by  $a$  and  $b$ , respectively, and then scaled by the total somatic conductance. This is identical to the steady-state response of an ORGaNIC (compare **Eq. 39** with **Eq. 9**) when the total somatic conductance is  $g_v = 1$ .

There are a variety of combinations of the various parameters of this model when the total somatic conductance is approximately equal to 1. Two particular interesting special cases correspond to when the modulators are both on (e.g., when the responses are dominated by the input drive), and when the modulators are both off (e.g., delay period). The first special case is:

For  $g_{vs} = 1$ ,  $a^+ \ll 1$ ,  $b^+ \ll 1$ ,  $R_a \geq 1$ ,  $R_b \geq 1$ :

$$g_v \approx 1 + \frac{a^+}{R_a} + \frac{b^+}{R_b} = \frac{R_a R_b + R_b a^+ + R_a b^+}{R_a R_b} . \quad (41)$$

$$\frac{1}{g_v} \approx \frac{R_a R_b}{R_a R_b + R_b a^+ + R_a b^+} \approx 1$$

The second special case is:

For  $g_{vs} = 1, a^+ \gg 1, b^+ \gg 1, R_a R_b \gg 1$ :

$$g_v \approx 1 + \frac{1}{R_a} + \frac{1}{R_b} = \frac{R_a R_b + 2}{R_a R_b} \quad . \quad (42)$$

$$\frac{1}{g_v} \approx \frac{R_a R_b}{R_a R_b + 2} \approx 1$$

This is, of course, a simplified model of pyramidal cells. There are two simplifications that are particularly suspect. First is that there is no leak conductance in the dendrites. We can think of  $g_{vs} = 1$  as the somatic leak conductance, but the shunt conductances in the dendrites must be allowed to go to zero to correctly implement ORGaNICs. The second approximation is that the input drive and recurrent drive are mediated by synaptic currents, not conductance changes. A push-pull arrangement of synaptic inputs can act like a current source (Carandini and Heeger, 1994). See also: <http://www.cns.nyu.edu/~david/handouts/membrane.pdf>. But doing so necessitates a high level of spontaneous activity so that increases in excitation are met with equal decreases in inhibition, and vice versa, whereas spontaneous activity in PFC is generally low. Synaptic inputs can also be approximated as current sources when the membrane potential remains far from the (excitatory and inhibitory) synaptic reversal potentials.

See Appendix for full details of the implementation.

## Discussion

ORGaNICs, although introduced as a computational theory of working memory, may be applicable also to models of motor preparation (e.g., as in **Fig. 7**), motor control, sensory processing, and other components of executive control (in addition to working memory, such as cognitive control). ORGaNICs can of course be stacked in layers such that the inputs to one ORGaNIC are the outputs from one or more other ORGaNICs. Particular stacked architectures encompass convolutional neural nets (i.e., deep nets) as a special case: specifically when the encoding/embedding weight matrices are convolutional and when the modulators are large ( $a = b \gg 0$ ) and the output responses are dominated by the input drive. Consequently, sensory processing, motor control, working memory (along with some other cognitive control and executive control functions, i.e., controlling attention) may all share a common canonical computational foundation.

ORGaNICs build on Heeger's Theory of Cortical Function (TCF) (Heeger, 2017) that offers a framework for understanding how the brain accomplishes three key functions: (i) inference: perception is nonconvex optimization that combines sensory input with prior expectation; (ii) exploration: inference relies on neural response variability to explore different possible interpretations; (iii) prediction: inference includes making predictions over a hierarchy of timescales. TCF has a single modulator for all of the neurons in each layer (like  $\lambda$  in **Eq. 7**) whereas ORGaNICs may have a separate pair of modulators ( $a_j$  and  $b_j$ ) for each neuron. ORGaNICs also have a more general form for the recurrent weight matrix. But TCF includes a feedback drive across the layers of a stacked architecture, in addition to the input drive and recurrent drive. TCF predicts that the brain changes states depending on the values of the modulators. In some states, neural responses are dominated by the feedforward drive and the theory is identical to a conventional feedforward model (e.g., deep net), thereby preserving all of the desirable features of those models. In other states, the theory is a generative model that constructs a sensory representation from an abstract representation, like memory recall. In still other

states, the theory combines prior expectation with sensory input, explores different possible perceptual interpretations of ambiguous sensory inputs, and predicts forward in time. The theory, therefore, offers an empirically testable framework for understanding how the cortex accomplishes inference, exploration, and prediction. TCF is derived from an energy function, very much like **Eq. 1**. Consequently, ORGaNICs may be stacked (like TCF) to include feedback connections and generative capability.

### Implications for neuroscience

- 1) There is a critical need for developing behavioral tasks that animal models are capable of learning, and that involve both maintaining and manipulating information over time. ORGaNICs (and other LSTMs) manage long-term dependencies between sensory inputs at different times, using a combination of gated integration (e.g., when  $b_j > 0$  and  $a_j = 0$ ) and reset (when  $a_j > b_j$ ). Typical delayed-response tasks like the memory-guided saccade task are appropriate for studying what psychologists call “short-term memory”, but they are weak probes for studying working memory (Atkinson and Shiffrin, 1968; Cowan, 1998; Cowan, 2008; Postle, 2015), because those tasks do not involve manipulation of information over time. Behavioral tasks that are popular in studies of decision making involve integration of noisy sensory information (Shadlen and Newsome, 2001; Brunton et al., 2013; Hanks et al., 2015) or integration of probabilistic cues (Yang and Shadlen, 2007); variants of these tasks (e.g., Gold and Shadlen, 2003; Purcell and Kiani, 2016) might be used to test the gated integration and reset functionality of ORGaNICs. The anti-saccade task (Hallett, 1978; Funahashi et al., 1993; Munoz and Everling, 2004; Johnston and Everling, 2006; Saber et al., 2015) and the double-step saccade task (Westheimer, 1954; Becker and Jurgens, 1979; Goldberg and Bruce, 1990; Medendorp et al., 2006; Medendorp et al., 2007) might also be used, with delay periods, to test the theory and to characterize how cortical circuits manage long-term dependencies.
- 2) Don’t be hung up about modulations of activity during a delay period. ORGaNICs, a straightforward extension of leaky neural integrators, can still be read out at any time during the delay in spite of the complicated dynamics. Indeed, we hypothesize that complicated dynamics is the norm, to support manipulation as well as maintenance.
- 3) Working memory and motor control may share a common computational foundation, and may be performed with the same circuit. Open-loop (i.e., ballistic) actions can be performed by initializing the state of an ORGaNIC (i.e., with the modulators turned on) from an input, and then by shutting off the modulators to let the dynamics play out. Closed-loop actions may also be performed with the same computation and circuit, in which the input drive reflects sensory feedback during the movement. This idea dovetails with experimental evidence demonstrating that motor cortical preparatory activity functions as advantageous initial conditions for subsequent peri-movement neural dynamics that generate the desired movement (Shenoy et al., 2013).
- 4) Examples of experimentally-testable predictions. First, the theory predicts that thalamic input changes the effective time constant and recurrent gain of a PFC neuron. Second, the specific biophysical implementation described above predicts that the soma and basal dendrites share input signals, but with opposite sign. This would, of course, have to be implemented with inhibitory interneurons.

### Implications for AI

- 1) Go complex. Simple harmonic motion is everywhere. For many applications (e.g.,

speech processing, music processing, analyzing human movement), the dynamics of the input signals may be characterized with damped oscillators, in which the amplitudes, frequencies and phases of the oscillators may change over time. The complex-valued weights and responses in ORGaNICs are well-suited for these kinds of signals. Likewise, damped-oscillator basis functions were proposed as a means for predicting forward in time (over a hierarchy of time scales) in our previous paper outlining a broad theory of cortical function (Heeger, 2017). Traditional LSTMs essentially approximate these modulated, oscillatory signals with piecewise constant functions. There are a few papers that suggest using complex-valued weights in RNNs (Widrow et al., 1975; Arjovsky et al., 2016; Danihelka et al., 2016; Wisdom et al., 2016; Jing et al., 2017; Jose et al., 2017), but not explicitly for the purpose of modeling simple harmonic motion, nor for modeling signals with damped oscillator basis functions.

- 2) Stability. To ensure stability and to avoid exploding gradients during learning, the recurrent weight matrix should be rescaled so that the eigenvalue with the largest real part is no larger than 1. This rescaling could be added as an extra step during learning after each gradient update. Avoid vanishing gradients by using rectification instead of saturating nonlinearities.
- 3) Effective time-constant and recurrent gain. The modulators in ORGaNICs control the effective time constant and recurrent gain. This characterization is complementary to the common description of LSTMs in terms of update gates and reset gates.
- 4) Neuromorphic implementation. Given the biophysical (equivalent electrical-circuit) implementation of ORGaNICs, it may be possible to design and fabricate analog VLSI ORGaNICs chips. Analog circuitry may be more energy-efficient in comparison to representing and processing information digitally (e.g., Mead, 1990; Sarpeshkar, 1998). Such an analog electrical-circuit may be configured to download various parameter settings (e.g., the weight matrices and offsets), computed separately offline.

### Learning

Left open is how to determine the weights in the various weight matrices: the encoding matrix ( $\mathbf{W}_{zx}$ ), the recurrent weight matrix ( $\mathbf{W}_{yy}$ ), the readout matrix ( $\mathbf{W}_{ry}$ ), the modulator weight matrices ( $\mathbf{W}_{ax}$ ,  $\mathbf{W}_{bx}$ ,  $\mathbf{W}_{ay}$ ,  $\mathbf{W}_{by}$ ), and the various offsets ( $\mathbf{c}_z$ ,  $\mathbf{c}_y$ ,  $\mathbf{c}_a$ ,  $\mathbf{c}_b$ ,  $\mathbf{c}_r$ ). A supervised learning approach would estimate the weights via gradient descent, given target values for the response time-courses (or the readout time-courses), if you have access to such target values sampled over time. Another approach would be to learn the weights via adaptive dynamic programming, i.e., the continuous-time equivalent of reinforcement learning (Murray et al., 2002; Lewis and Vrabie, 2009; Wang et al., 2009; e.g., Yu et al., 2017). Yet another approach would be an unsupervised learning algorithm based on minimizing prediction error over time (Heeger, 2017).

## Appendix: Biophysical implementation

### Thalamus

The responses of the modulators (**a** and **b**) were presumed to be computed by neurons in thalamus (Guo et al., 2017; Schmitt et al., 2017). Each neuron was modeled as a single-compartment electrical circuit with conductance-based synapses. We start with the membrane equation:

$$C \frac{dv}{dt} = -g_l(v - E_l) - g_e(v - E_e) - g_i(v - E_i) , \quad (43)$$

The leak conductance, excitatory synaptic conductance, and inhibitory synaptic conductance, are denoted  $g_l$ ,  $g_e$ , and  $g_i$ , respectively. The corresponding reversal potentials are denoted  $E_l$ ,  $E_e$ , and  $E_i$ . To simplify the notation (without loss of generality), we choose  $E_l = 0$ ,  $E_e = 1$ , and  $E_i = -1$ . Rewriting Eq. 43:

$$\begin{aligned} C \frac{dv}{dt} &= -(g_l + g_e + g_i)v + g_e - g_i \\ \tau \frac{dv}{dt} &= -v + \frac{g_e - g_i}{g} \end{aligned} , \quad (44)$$

where we define:

$$g = (g_l + g_e + g_i) \quad (45)$$

$$\tau = \frac{C}{g} . \quad (46)$$

To compute a linear summation of inputs  $\mathbf{x}$  following by a saturating nonlinearity, we specify the synaptic conductances:

$$\begin{aligned} g_e &= \sum_k w_k^+ x_k^+ + w_k^- x_k^- \\ g_i &= \sum_k w_k^+ x_k^- + w_k^- x_k^+ \end{aligned} , \quad (47)$$

where  $w_k$  are the weights in the weighted sum, and where the superscript + and - mean halfwave rectification:

$$x_k^+ = \lfloor x_k \rfloor \text{ and } x_k^- = \lfloor -x_k \rfloor . \quad (48)$$

Subtracting the two lines of Eq. 47 gives linear summation:

$$\begin{aligned} g_e - g_i &= \sum_k w_k^+ x_k^+ + w_k^- x_k^- - w_k^+ x_k^- - w_k^- x_k^+ \\ &= \sum_k (w_k^+ - w_k^-) x_k^+ - (w_k^+ - w_k^-) x_k^- \\ &= \sum_k w_k x_k^+ - w_k x_k^- \\ &= \sum_k w_k x_k \end{aligned} . \quad (49)$$

Substituting from **Eq. 49** into **Eq. 44** and solving for the steady state responses gives linear summation followed by a saturating nonlinearity:

$$v = \frac{g_e - g_i}{g} = \frac{1}{g} \sum_k w_k x_k . \quad (50)$$

The dynamic, time-varying responses of the full population of thalamic neurons was implemented as follows:

$$\begin{aligned} \mathbf{x}^+ &= \lfloor \mathbf{x} \rfloor \text{ and } \mathbf{x}^- = \lfloor -\mathbf{x} \rfloor \\ \mathbf{y}^+ &= \lfloor \mathbf{y} \rfloor \text{ and } \mathbf{y}^- = \lfloor -\mathbf{y} \rfloor \end{aligned} \quad (51)$$

$$\begin{aligned} \mathbf{a}^+ &= \lfloor \mathbf{a} \rfloor \text{ and } \mathbf{a}^- = \lfloor -\mathbf{a} \rfloor \\ \mathbf{W}_{ax}^+ &= \lfloor \mathbf{W}_{ax} \rfloor \text{ and } \mathbf{W}_{ax}^- = \lfloor -\mathbf{W}_{ax} \rfloor \\ \mathbf{W}_{ay}^+ &= \lfloor \mathbf{W}_{ay} \rfloor \text{ and } \mathbf{W}_{ay}^- = \lfloor -\mathbf{W}_{ay} \rfloor \\ \mathbf{c}_a^+ &= \lfloor \mathbf{c}_a \rfloor \text{ and } \mathbf{c}_a^- = \lfloor -\mathbf{c}_a \rfloor \end{aligned} \quad (52)$$

$$\begin{aligned} \mathbf{b}^+ &= \lfloor \mathbf{b} \rfloor \text{ and } \mathbf{b}^- = \lfloor -\mathbf{b} \rfloor \\ \mathbf{W}_{bx}^+ &= \lfloor \mathbf{W}_{bx} \rfloor \text{ and } \mathbf{W}_{bx}^- = \lfloor -\mathbf{W}_{bx} \rfloor \\ \mathbf{W}_{by}^+ &= \lfloor \mathbf{W}_{by} \rfloor \text{ and } \mathbf{W}_{by}^- = \lfloor -\mathbf{W}_{by} \rfloor \\ \mathbf{c}_b^+ &= \lfloor \mathbf{c}_b \rfloor \text{ and } \mathbf{c}_b^- = \lfloor -\mathbf{c}_b \rfloor \end{aligned} \quad (53)$$

$$\begin{aligned} \Delta \mathbf{a}(t) &= \frac{\Delta t}{C} [-\mathbf{g}_a(t)\mathbf{a}(t) + \mathbf{g}_{ea}(t) - \mathbf{g}_{ia}(t)] \\ \mathbf{a}(t + \Delta t) &= \mathbf{a}(t) + \Delta \mathbf{a}(t) \\ \mathbf{g}_{ea}(t) &= \mathbf{W}_{ax}^+ \mathbf{x}^+(t) + \mathbf{W}_{ax}^- \mathbf{x}^-(t) + \mathbf{W}_{ay}^+ \mathbf{y}^+(t) + \mathbf{W}_{ay}^- \mathbf{y}^-(t) + \mathbf{c}_a^+ \\ \mathbf{g}_{ia}(t) &= \mathbf{W}_{ax}^- \mathbf{x}^+(t) + \mathbf{W}_{ax}^+ \mathbf{x}^-(t) + \mathbf{W}_{ay}^- \mathbf{y}^+(t) + \mathbf{W}_{ay}^+ \mathbf{y}^-(t) + \mathbf{c}_a^- \\ \mathbf{g}_a(t) &= \mathbf{g}_{ea}(t) + \mathbf{g}_{ia}(t) + g_l \end{aligned} \quad (54)$$

$$\begin{aligned} \Delta \mathbf{b}(t) &= \frac{\Delta t}{C} [-\mathbf{g}_b(t)\mathbf{b}(t) + \mathbf{g}_{eb}(t) - \mathbf{g}_{ib}(t)] \\ \mathbf{b}(t + \Delta t) &= \mathbf{b}(t) + \Delta \mathbf{b}(t) \\ \mathbf{g}_{eb}(t) &= \mathbf{W}_{bx}^+ \mathbf{x}^+(t) + \mathbf{W}_{bx}^- \mathbf{x}^-(t) + \mathbf{W}_{by}^+ \mathbf{y}^+(t) + \mathbf{W}_{by}^- \mathbf{y}^-(t) + \mathbf{c}_b^+ \\ \mathbf{g}_{ib}(t) &= \mathbf{W}_{bx}^- \mathbf{x}^+(t) + \mathbf{W}_{bx}^+ \mathbf{x}^-(t) + \mathbf{W}_{by}^- \mathbf{y}^+(t) + \mathbf{W}_{by}^+ \mathbf{y}^-(t) + \mathbf{c}_b^- \\ \mathbf{g}_b(t) &= \mathbf{g}_{eb}(t) + \mathbf{g}_{ib}(t) + g_l \end{aligned} \quad (55)$$

PFC

The dynamic, time-varying responses of the full population of PFC neurons was implemented as follows:

$$\begin{aligned}\mathbf{y}^+(t) &= \lfloor \mathbf{v}^+(t) \rfloor \\ \mathbf{y}^-(t) &= \lfloor \mathbf{v}^-(t) \rfloor\end{aligned}\tag{56}$$

$$\begin{aligned}\mathbf{W}_{zx}^+ &= \lfloor \mathbf{W}_{zx} \rfloor \text{ and } \mathbf{W}_{zx}^- = \lfloor -\mathbf{W}_{zx} \rfloor \\ \mathbf{c}_z^+ &= \lfloor \mathbf{c}_z \rfloor \text{ and } \mathbf{c}_z^- = \lfloor -\mathbf{c}_z \rfloor\end{aligned}\tag{57}$$

$$\begin{aligned}\mathbf{W}_{\hat{y}y}^+ &= \lfloor \mathbf{W}_{\hat{y}y} \rfloor \text{ and } \mathbf{W}_{\hat{y}y}^- = \lfloor -\mathbf{W}_{\hat{y}y} \rfloor \\ \mathbf{c}_{\hat{y}}^+ &= \lfloor \mathbf{c}_{\hat{y}} \rfloor \text{ and } \mathbf{c}_{\hat{y}}^- = \lfloor -\mathbf{c}_{\hat{y}} \rfloor\end{aligned}\tag{58}$$

$$\begin{aligned}\Delta \mathbf{v}^+(t) &= \frac{\Delta t}{C} \left[ -g_{vs} \mathbf{v}^+(t) + (\mathbf{I}_z^+(t) - \mathbf{I}_z^-(t)) + \mathbf{I}_{as}^+(t) + \mathbf{I}_{bs}^+(t) \right] \\ \mathbf{v}^+(t + \Delta t) &= \mathbf{v}^+(t) + \Delta \mathbf{v}^+(t) \\ \Delta \mathbf{v}_a^+(t) &= \frac{\Delta t}{C} \left[ -\mathbf{g}_{va}(t) \odot \mathbf{v}_a^+(t) + (\mathbf{I}_{\hat{y}}^+(t) - \mathbf{I}_{\hat{y}}^-(t)) - \mathbf{I}_{as}^+(t) \right] \\ \mathbf{v}_a^+(t + \Delta t) &= \mathbf{v}_a^+(t) + \Delta \mathbf{v}_a^+(t) \\ \Delta \mathbf{v}_b^+(t) &= \frac{\Delta t}{C} \left[ -\mathbf{g}_{vb}(t) \odot \mathbf{v}_b^+(t) + (\mathbf{I}_z^-(t) - \mathbf{I}_z^+(t)) - \mathbf{I}_{bs}^+(t) \right] \\ \mathbf{v}_b^+(t + \Delta t) &= \mathbf{v}_b^+(t) + \Delta \mathbf{v}_b^+(t)\end{aligned}\tag{59}$$

$$\begin{aligned}\Delta \mathbf{v}^-(t) &= \frac{\Delta t}{C} \left[ -g_{vs} \mathbf{v}^-(t) + (\mathbf{I}_z^-(t) - \mathbf{I}_z^+(t)) + \mathbf{I}_{as}^-(t) + \mathbf{I}_{bs}^-(t) \right] \\ \mathbf{v}^-(t + \Delta t) &= \mathbf{v}^-(t) + \Delta \mathbf{v}^-(t) \\ \Delta \mathbf{v}_a^-(t) &= \frac{\Delta t}{C} \left[ -\mathbf{g}_{va}(t) \odot \mathbf{v}_a^-(t) + (\mathbf{I}_{\hat{y}}^-(t) - \mathbf{I}_{\hat{y}}^+(t)) - \mathbf{I}_{as}^-(t) \right] \\ \mathbf{v}_a^-(t + \Delta t) &= \mathbf{v}_a^-(t) + \Delta \mathbf{v}_a^-(t) \\ \Delta \mathbf{v}_b^-(t) &= \frac{\Delta t}{C} \left[ -\mathbf{g}_{vb}(t) \odot \mathbf{v}_b^-(t) + (\mathbf{I}_z^+(t) - \mathbf{I}_z^-(t)) - \mathbf{I}_{bs}^-(t) \right] \\ \mathbf{v}_b^-(t + \Delta t) &= \mathbf{v}_b^-(t) + \Delta \mathbf{v}_b^-(t)\end{aligned}\tag{60}$$

$$\begin{aligned}\mathbf{g}_{va}(t) &= \frac{1}{R_a} \mathbf{a}^+(t) \\ \mathbf{g}_{vb}(t) &= \frac{1}{R_b} \mathbf{b}^+(t)\end{aligned}\tag{61}$$

$$\begin{aligned}\mathbf{I}_z^+(t) &= \mathbf{W}_{zx}^+ x^+(t) + \mathbf{W}_{zx}^- x^-(t) + \mathbf{c}_z^+ \\ \mathbf{I}_z^-(t) &= \mathbf{W}_{zx}^- x^+(t) + \mathbf{W}_{zx}^+ x^-(t) + \mathbf{c}_z^-\end{aligned}\tag{62}$$

$$\begin{aligned}\mathbf{I}_{\hat{y}}^+(t) &= \mathbf{W}_{\hat{y}y}^+ y^+(t) + \mathbf{W}_{\hat{y}y}^- y^-(t) + \mathbf{c}_{\hat{y}}^+ \\ \mathbf{I}_{\hat{y}}^-(t) &= \mathbf{W}_{\hat{y}y}^- y^+(t) + \mathbf{W}_{\hat{y}y}^+ y^-(t) + \mathbf{c}_{\hat{y}}^-\end{aligned}\tag{63}$$

$$\begin{aligned}\mathbf{I}_{as}^+(t) &= \frac{1}{R_a} (\mathbf{v}_a^+(t) - \mathbf{v}^+(t)) \\ \mathbf{I}_{as}^-(t) &= \frac{1}{R_a} (\mathbf{v}_a^-(t) - \mathbf{v}^-(t))\end{aligned}\tag{64}$$

$$\begin{aligned}\mathbf{I}_{bs}^+(t) &= \frac{1}{R_b} (\mathbf{v}_b^+(t) - \mathbf{v}^+(t)) \\ \mathbf{I}_{bs}^-(t) &= \frac{1}{R_b} (\mathbf{v}_b^-(t) - \mathbf{v}^-(t))\end{aligned}\tag{65}$$

The circle-dot notation  $\odot$  means element-wise multiplication.

The firing rates ( $\mathbf{y}^+$  and  $\mathbf{y}^-$ ), synaptic weights ( $\mathbf{W}^+$  and  $\mathbf{W}^-$ ) and offsets ( $\mathbf{c}^+$  and  $\mathbf{c}^-$ ), shunting conductances ( $g_{va}$  and  $g_{vb}$ ), and synaptic currents ( $\mathbf{I}_z^+$ ,  $\mathbf{I}_z^-$ ,  $\mathbf{I}_{\hat{y}}^+$ ,  $\mathbf{I}_{\hat{y}}^-$ ) are all non-negative, because of the rectifying nonlinearities. The internal currents ( $\mathbf{I}_{as}^+$ ,  $\mathbf{I}_{as}^-$ ,  $\mathbf{I}_{bs}^+$ ,  $\mathbf{I}_{bs}^-$ ) may be positive or negative, depending on whether current is flowing toward or away from the soma. The minus signs in **Eqs. 59** and **60** may be implemented with inhibitory interneurons that flip the sign by having a hyperpolarizing reversal potential.

And we're done! Phew...

## References

Abeles M (1982) Local Cortical Circuits: An Electrophysiological Study: Springer-Verlag.

Almeida R, Barbosa J, Compte A (2015) Neural circuit basis of visuo-spatial working memory precision: a computational and behavioral study. *J Neurophysiol* 114:1806-1818.

Arjovsky M, Shah A, Bengio Y (2016) Unitary evolution recurrent neural networks. In: International Conference on Machine Learning, pp 1120-1128.

Assael YM, Shillingford B, Whiteson S, de Freitas N (2016) Lipnet: Sentence-level lipreading. arXiv preprint arXiv:161101599.

Atkinson RC, Shiffrin RM (1968) Human memory: A proposed system and its control processes1. In: Psychology of learning and motivation, pp 89-195: Elsevier.

Becker W, Jurgens R (1979) An analysis of the saccadic system by means of double step stimuli. *Vision Res* 19:967-983.

Brody CD, Hernandez A, Zainos A, Romo R (2003) Timing and neural encoding of somatosensory parametric working memory in macaque prefrontal cortex. *Cereb Cortex* 13:1196-1207.

Brunton BW, Botvinick MM, Brody CD (2013) Rats and humans can optimally accumulate evidence for decision-making. *Science* 340:95-98.

Carandini M, Heeger DJ (1994) Summation and division by neurons in primate visual cortex. *Science* 264:1333-1336.

Carandini M, Heeger DJ (2012) Normalization as a canonical neural computation. *Nat Rev Neurosci* 13:51-62.

Chan W, Jaitly N, Le Q, Vinyals O (2016) Listen, attend and spell: A neural network for large vocabulary conversational speech recognition. In: Acoustics, Speech and Signal Processing (ICASSP), 2016 IEEE International Conference on, pp 4960-4964: IEEE.

Cho K, Van Merriënboer B, Gulcehre C, Bahdanau D, Bougares F, Schwenk H, Bengio Y (2014) Learning phrase representations using RNN encoder-decoder for statistical machine translation. arXiv preprint arXiv:14061078.

Chorowski JK, Bahdanau D, Serdyuk D, Cho K, Bengio Y (2015) Attention-based models for speech recognition. In: Advances in neural information processing systems, pp 577-585.

Compte A, Brunel N, Goldman-Rakic PS, Wang XJ (2000) Synaptic mechanisms and network dynamics underlying spatial working memory in a cortical network model. *Cereb Cortex* 10:910-923.

Constantinidis C, Williams GV, Goldman-Rakic PS (2002) A role for inhibition in shaping the temporal flow of information in prefrontal cortex. *Nat Neurosci* 5:175-180.

Costa R, Assael IA, Shillingford B, de Freitas N, Vogels T (2017) Cortical microcircuits as gated-recurrent neural networks. In: Advances in Neural Information Processing Systems, pp 272-283.

Cowan N (1998) Attention and memory: An integrated framework: Oxford University Press.

Cowan N (2008) What are the differences between long-term, short-term, and working memory? *Prog Brain Res* 169:323-338.

Danihelka I, Wayne G, Uria B, Kalchbrenner N, Graves A (2016) Associative long short-term memory. arXiv preprint arXiv:160203032.

Funahashi S, Bruce CJ, Goldman-Rakic PS (1989) Mnemonic coding of visual space in the monkey's dorsolateral prefrontal cortex. *J Neurophysiol* 61:331-349.

Funahashi S, Chafee MV, Goldman-Rakic PS (1993) Prefrontal neuronal activity in rhesus monkeys performing a delayed anti-saccade task. *Nature* 365:753-756.

Fuster JM (1973) Unit activity in prefrontal cortex during delayed-response performance: neuronal correlates of transient memory. *J Neurophysiol* 36:61-78.

Fuster JM, Alexander GE (1971) Neuron activity related to short-term memory. *Science* 173:652-654.

Gnadt JW, Andersen RA (1988) Memory related motor planning activity in posterior parietal cortex of macaque. *Experimental Brain Research* 70:216-220.

Gold JI, Shadlen MN (2003) The influence of behavioral context on the representation of a perceptual decision in developing oculomotor commands. *J Neurosci* 23:632-651.

Goldberg ME, Bruce CJ (1990) Primate frontal eye fields. III. Maintenance of a spatially accurate saccade signal. *J Neurophysiol* 64:489-508.

Goldman MS (2009) Memory without feedback in a neural network. *Neuron* 61:621-634.

Goldman-Rakic PS (1995) Cellular basis of working memory. *Neuron* 14:477-485.

Graves A (2013) Generating sequences with recurrent neural networks. arXiv preprint arXiv:13080850.

Graves A, Mohamed A-r, Hinton G (2013) Speech recognition with deep recurrent neural networks. In: *Acoustics, speech and signal processing (icassp), 2013 ieee international conference on*, pp 6645-6649: IEEE.

Graves A, Wayne G, Danihelka I (2014) Neural turing machines. arXiv preprint arXiv: 14105401.

Guo ZV, Inagaki HK, Daie K, Druckmann S, Gerfen CR, Svoboda K (2017) Maintenance of persistent activity in a frontal thalamocortical loop. *Nature* 545:181-186.

Hallett PE (1978) Primary and secondary saccades to goals defined by instructions. *Vision Res* 18:1279-1296.

Hanks TD, Kopec CD, Brunton BW, Duan CA, Erlich JC, Brody CD (2015) Distinct relationships of parietal and prefrontal cortices to evidence accumulation. *Nature* 520:220-223.

Hasegawa R, Sawaguchi T, Kubota K (1998) Monkey prefrontal neuronal activity coding the forthcoming saccade in an oculomotor delayed matching-to-sample task. *J Neurophysiol* 79:322-333.

Heeger DJ (1992a) Half-squaring in responses of cat striate cells. *Vis Neurosci* 9:427-443.

Heeger DJ (1992b) Normalization of cell responses in cat striate cortex. *Vis Neurosci* 9:181-197.

Heeger DJ (2017) Theory of cortical function. *Proc Natl Acad Sci U S A* 114:1773-1782.

Hochreiter S, Schmidhuber J (1997) Long short-term memory. *Neural Comput* 9:1735-1780.

Hochreiter S, Bengio Y, Frasconi P, Schmidhuber J (2001) Gradient flow in recurrent nets: the difficulty of learning long-term dependencies. In: A field guide to dynamical recurrent neural networks. IEEE Press.

Hussar CR, Pasternak T (2012) Memory-guided sensory comparisons in the prefrontal cortex: contribution of putative pyramidal cells and interneurons. *J Neurosci* 32:2747-2761.

Jacobsen CF (1935) Functions of frontal association area in primates. *Archives of Neurology & Psychiatry* 33:558-569.

Janssen P, Shadlen MN (2005) A representation of the hazard rate of elapsed time in macaque area LIP. *Nat Neurosci* 8:234-241.

Jing L, Gulcehre C, Peurifoy J, Shen Y, Tegmark M, Soljačić M, Bengio Y (2017) Gated orthonormal recurrent units: On learning to forget. *arXiv preprint arXiv:170602761*.

Johnston K, Everling S (2006) Neural activity in monkey prefrontal cortex is modulated by task context and behavioral instruction during delayed-match-to-sample and conditional prosaccade-antisaccade tasks. *J Cogn Neurosci* 18:749-765.

Jose C, Cisse M, Fleuret F (2017) Kronecker Recurrent Units. *arXiv preprint arXiv:170510142*.

Kobak D, Brendel W, Constantinidis C, Feierstein CE, Kepcs A, Mainen ZF, Qi XL, Romo R, Uchida N, Machens CK (2016) Demixed principal component analysis of neural population data. *Elife* 5.

Lebedev MA, Messinger A, Kralik JD, Wise SP (2004) Representation of attended versus remembered locations in prefrontal cortex. *PLoS Biol* 2:e365.

Lewis FL, Vrabie D (2009) Reinforcement learning and adaptive dynamic programming for feedback control. *IEEE circuits and systems magazine* 9.

Lundqvist M, Compte A, Lansner A (2010) Bistable, irregular firing and population oscillations in a modular attractor memory network. *PLoS Comput Biol* 6:e1000803.

Lundqvist M, Herman P, Lansner A (2011) Theta and gamma power increases and alpha/beta power decreases with memory load in an attractor network model. *J Cogn Neurosci* 23:3008-3020.

Lundqvist M, Rose J, Herman P, Brincat SL, Buschman TJ, Miller EK (2016) Gamma and Beta Bursts Underlie Working Memory. *Neuron* 90:152-164.

Machens CK, Romo R, Brody CD (2005) Flexible control of mutual inhibition: a neural model of two-interval discrimination. *Science* 307:1121-1124.

Markowitz DA, Curtis CE, Pesaran B (2015) Multiple component networks support working memory in prefrontal cortex. *Proc Natl Acad Sci U S A* 112:11084-11089.

Mead C (1990) Neuromorphic Electronic Systems. *Proceedings of the Ieee* 78:1629-1636.

Medendorp WP, Goltz HC, Vilis T (2006) Directional selectivity of BOLD activity in human posterior parietal cortex for memory-guided double-step saccades. *J Neurophysiol* 95:1645-1655.

Medendorp WP, Kramer GF, Jensen O, Oostenveld R, Schoffelen JM, Fries P (2007) Oscillatory activity in human parietal and occipital cortex shows hemispheric lateralization and memory effects in a delayed double-step saccade task. *Cereb Cortex* 17:2364-2374.

Messinger A, Lebedev MA, Kralik JD, Wise SP (2009) Multitasking of attention and memory functions in the primate prefrontal cortex. *J Neurosci* 29:5640-5653.

Munoz DP, Everling S (2004) Look away: the anti-saccade task and the voluntary control of eye movement. *Nat Rev Neurosci* 5:218-228.

Murray JD, Bernacchia A, Roy NA, Constantinidis C, Romo R, Wang XJ (2017) Stable population coding for working memory coexists with heterogeneous neural dynamics in prefrontal cortex. *Proc Natl Acad Sci U S A* 114:394-399.

Murray JJ, Cox CJ, Lendaris GG, Saeks R (2002) Adaptive dynamic programming. *IEEE Transactions on Systems, Man, and Cybernetics, Part C (Applications and Reviews)* 32:140-153.

O'Reilly RC, Frank MJ (2006) Making working memory work: a computational model of learning in the prefrontal cortex and basal ganglia. *Neural Comput* 18:283-328.

Pascanu R, Mikolov T, Bengio Y (2013) On the difficulty of training recurrent neural networks. In: *International Conference on Machine Learning*, pp 1310-1318.

Pesaran B, Pezaris JS, Sahani M, Mitra PP, Andersen RA (2002) Temporal structure in neuronal activity during working memory in macaque parietal cortex. *Nat Neurosci* 5:805-811.

Platt ML, Glimcher PW (1999) Neural correlates of decision variables in parietal cortex. *Nature* 400:233-238.

Postle BR (2015) The cognitive neuroscience of visual short-term memory. *Curr Opin Behav Sci* 1:40-46.

Purcell BA, Kiani R (2016) Hierarchical decision processes that operate over distinct timescales underlie choice and changes in strategy. *Proc Natl Acad Sci U S A* 113:E4531-4540.

Quintana J, Fuster JM (1992) Mnemonic and predictive functions of cortical neurons in a memory task. *Neuroreport* 3:721-724.

Romo R, Brody CD, Hernandez A, Lemus L (1999) Neuronal correlates of parametric working memory in the prefrontal cortex. *Nature* 399:470-473.

Rowe JB, Toni I, Josephs O, Frackowiak RS, Passingham RE (2000) The prefrontal cortex: response selection or maintenance within working memory? *Science* 288:1656-1660.

Saber GT, Pestilli F, Curtis CE (2015) Saccade planning evokes topographically specific activity in the dorsal and ventral streams. *J Neurosci* 35:245-252.

Sarpeshkar R (1998) Analog versus digital: extrapolating from electronics to neurobiology. *Neural Comput* 10:1601-1638.

Schluppeck D, Curtis CE, Glimcher PW, Heeger DJ (2006) Sustained activity in topographic areas of human posterior parietal cortex during memory-guided saccades. *J Neurosci* 26:5098-5108.

Schmitt LI, Wimmer RD, Nakajima M, Happ M, Mofakham S, Halassa MM (2017) Thalamic amplification of cortical connectivity sustains attentional control. *Nature* 545:219-223.

Shadlen MN, Newsome WT (2001) Neural basis of a perceptual decision in the parietal cortex (area LIP) of the rhesus monkey. *J Neurophysiol* 86:1916-1936.

Shafi M, Zhou Y, Quintana J, Chow C, Fuster J, Bodner M (2007) Variability in neuronal ac-

tivity in primate cortex during working memory tasks. *Neuroscience* 146:1082-1108.

Shenoy KV, Sahani M, Churchland MM (2013) Cortical control of arm movements: a dynamical systems perspective. *Annual review of neuroscience* 36:337-359.

Srimal R, Curtis CE (2008) Persistent neural activity during the maintenance of spatial position in working memory. *Neuroimage* 39:455-468.

Sutskever I, Vinyals O, Le QV (2014) Sequence to sequence learning with neural networks. In: *Advances in neural information processing systems*, pp 3104-3112.

van den Oord A, Kalchbrenner N, Espeholt L, Vinyals O, Graves A (2016) Conditional image generation with pixelcnn decoders. In: *Advances in Neural Information Processing Systems*, pp 4790-4798.

Wang F-Y, Zhang H, Liu D (2009) Adaptive dynamic programming: An introduction. *IEEE computational intelligence magazine* 4.

Wang XJ (1999) Synaptic basis of cortical persistent activity: the importance of NMDA receptors to working memory. *J Neurosci* 19:9587-9603.

Wang XJ (2001) Synaptic reverberation underlying mnemonic persistent activity. *Trends Neurosci* 24:455-463.

Watanabe M (1996) Reward expectancy in primate prefrontal neurons. *Nature* 382:629-632.

Westheimer G (1954) Eye movement responses to a horizontally moving visual stimulus. *AMA Arch Ophthalmol* 52:932-941.

Widrow B, McCool J, Ball M (1975) The complex LMS algorithm. *Proceedings of the IEEE* 63:719-720.

Wimmer K, Nykamp DQ, Constantinidis C, Compte A (2014) Bump attractor dynamics in prefrontal cortex explains behavioral precision in spatial working memory. *Nat Neurosci* 17:431-439.

Wisdom S, Powers T, Hershey J, Le Roux J, Atlas L (2016) Full-capacity unitary recurrent neural networks. In: *Advances in Neural Information Processing Systems*, pp 4880-4888.

Yang T, Shadlen MN (2007) Probabilistic reasoning by neurons. *Nature* 447:1075-1080.

Yu H, Jiang Y, Jiang Z-P (2017) Robust Adaptive Dynamic Programming: John Wiley & Sons.